ISSN 1075-7015, Geology of Ore Deposits, 2017, Vol. 59, No. 6, pp. 453–481. © Pleiades Publishing, Ltd., 2017.
Original Russian Text © A.A. Kalinin, O.V. Kazanov, N.M. Kudryashov, G.F. Bakaev, S.V. Petrov, D.V. Elizarov, L.V. Lyalina, 2017, published in Geologiya Rudnykh Mestorozhdenii, 2017, Vol. 59, No. 6, pp. 470–500.

New Promising Gold-Ore Objects in the Strelna Greenstone Belt, Kola Peninsula

A. A. Kalinin[a], *, O. V. Kazanov[b], N. M. Kudryashov[a], G. F. Bakaev[b], S. V. Petrov[c], D. V. Elizarov[a], and L. V. Lyalina[a]

[a]*Geological Institute, Kola Science Center, Russian Academy of Sciences, Apatity, 184209 Russia*
[b]*Central Kola Expedition, Monchegorsk, 184500 Russia*
[c]*St. Petersburg State University, St. Petersburg, 199034 Russia*
**e-mail: kalinin@geoksc.apatity.ru*

Received June 29, 2015

Abstract—Data on gold ore objects in the Strelna Greenstone Belt in the southeastern Kola Peninsula are presented in the paper. The studied Vorgovy and Sergozero ore occurrences are localized in the zone of tectonic contact of the Neoarchean complexes making up the greenstone belt and the volcanic–sedimentary sequences of the Paleoproterozoic Imandra–Varzuga Zone. The Vorgovy gold occurrence is related to stockwork of carbonate–quartz veins and veinlets hosted in a biotite gneiss transformed into chlorite–sericite–quartz metasomatic rock with pyrrhotite–arsenopyrite dissemination. The Sergozero occurrence is localized in amphibolites corresponding to komatiitic and tholeiitic basalts hosted in biotite gneiss (metapelite). Mineralization is confined to the zone of tectonized contact between komatiitic and tholeiitic basalts, where it is controlled by a strip of metasomatic biotite–calcite rock with gersdorffite–arsenopyrite dissemination. The native gold grains medium to high in fineness are up to 0.1 mm in size and mainly localized at the contact of arsenopyrite and gersdorffite with gangue minerals. Gold mineralization is of superimposed character, and, as indicated by isotopic geochronology, was formed at the retrograde stage of the Svecofennian regional metamorphism. Comparison of ore occurrences localized in the Strelna Greenstone Belt with gold deposits in greenstone belts of the western Fennoscandian Shield and the Superior Province in Canada allows us to suggest a high perspective of the entire Strelna Belt for gold.

DOI: 10.1134/S1075701517060022

INTRODUCTION

The Strelna Greenstone Belt (SGB) is situated in the southeastern part of Kola Peninsula (Fig. 1). This part of the region is distinguished by a complex geological structure and remains poorly studied because of its remoteness from settlements and roads in combination with the waterlogging area almost completely devoid of outcrops (Fig. 2). The complicated physicogeographic conditions predetermine the technique of prospecting for gold, which is comprised of the geochemical survey of middle SGB using till sampling (survey on the basis of secondary haloes at the glacial sediments bottom), which was well demonstrated in prospecting under similar conditions in Finland (Nurmi, 1991) with the following verification of revealed geochemical anomalies by drilling of boreholes. Almost all geological information on the Sergozero area presented in this paper has been obtained by drilling, documentation, and sampling of bore cores carried out by the Central Kola Expedition in perspective areas at the headwater of the Bol'shaya Varzuga River. Despite a limited volume of the performed works, their results yielded new information on volcanic–sedimentary complexes making up SGB and ore occurrences within the studied area. The largest gold object of a new genetic type for the northeastern Fennoscandian Shield has been discovered in the Kola region.

STRELNA GREENSTONE BELT

The SGB enters into the system of greenstone belts that extend along the southern boundary of the Paleoproterozoic Imandra–Varzuga Zone (IVZ). A toponymy of belt names was not formed for the time being because of insufficient data on geology of this part of the Fennoscandian Shield. Vrevsky et al. (2003) recognize here the Tersky and Ingozero structures of the Tersky–Allarechka Greenstone Belt. In the collective monograph published by M.V. Mints et al. (*Glubinnoe stroenie* ..., 2010), the Strelna and the Voche–Lambina belts are considered. They correspond to the Tersky structure (according to A.B. Vrevsky) and the Ingozero structure. Astaf'ev et al. (2010, 2012) use the term Tersky Belt for the whole tract of Neoarchean greenstone rocks along the southern boundary of IVZ from

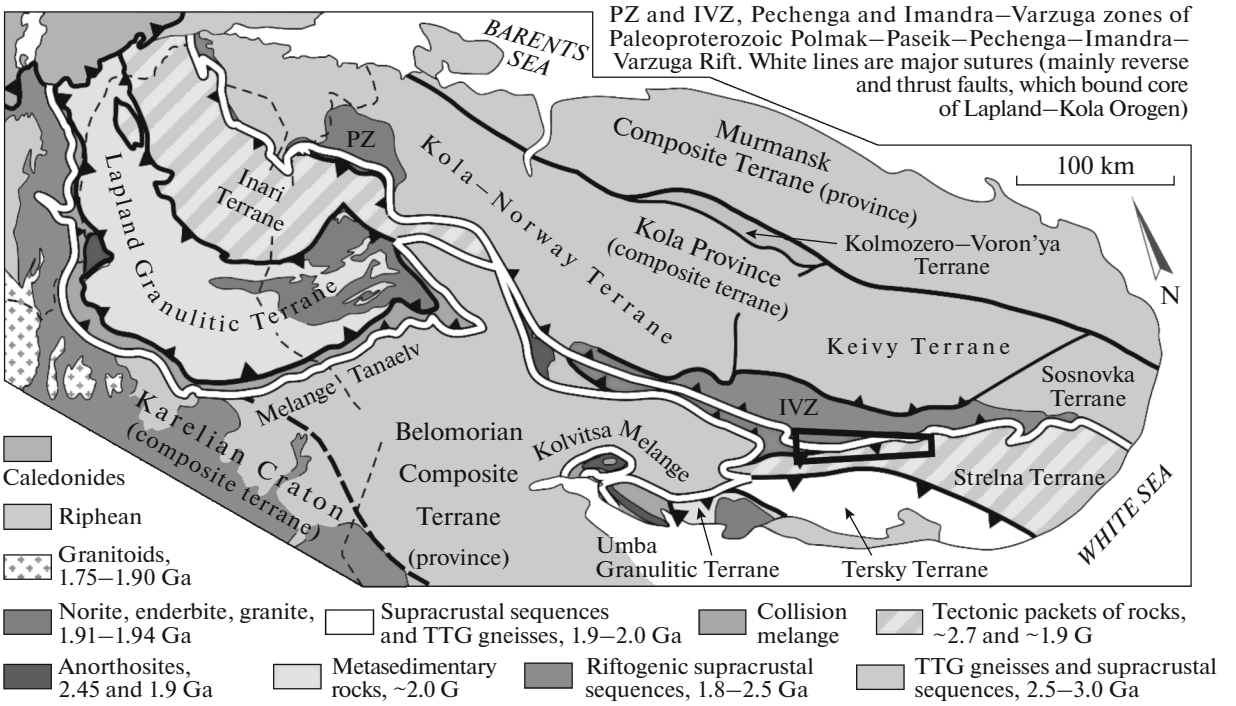

Fig. 1. Area of work (rectangle) in the schematic map of tectonic regionalization of the northeastern Baltic Shield. According to Balagansky et al. (2006).

Fig. 2. View on Greater Varzuga River valley in area of work.

Lake Imandra to the Throat of the White Sea; the Strelna segment is its eastern part. In this paper, we will adhere to the name of *Strelna Greenstone Belt* as the eastern part of greenstone belt system from the middle reaches of the Varzuga River to the eastern coast of Kola Peninsula within limits of the Strelna Terrane. The belt is ~170 km in extent, and its maximum width reaches ~40 km near the Sergozero–Babozero district.

The SGB occurs in the northern part of Strelna Terrane of Belomorian Province in the Fennoscandian Shield (Fig. 1). In the opinion of M.V. Mints et al. (*Glubinnoe stroenie* ..., 2010), the SGB is the Neoarchean (2.72–2.76 Ma) riftogenic trough formed in the eastern part of Kola microcontinent and filled with paragneisses, schists, and felsic and mafic metavolcanic rocks with komatiites subordinate in amount. The contemporary structural pattern of SGB was created to a significant measure in the Paleoproterozoic, when intracontinental collision took place with the formation of the Lapland–Kola–Belomorian Orogen (1.87–1.70 Ga ago) (*Glubinnoe stroenie* ..., 2010). According to the geodynamic model accepted during the last decade, the Strelna Terrane is a constituent of the core of Paleoproterozoic Lapland–Kola Orogen, whereas the Imandra–Varzuga Paleorift Zone situated to the north is related to the northeastern foreland of this orogen, which is named the Kola Composite Terrane (Fig. 1). The sequences of Strelna Terrane have been upthrown from the south over the Imandra–Varzuga Paleorift Zone (Balagansky et al., 2006; Daly et al., 2006); the tectonic boundary between SGB and IVZ is traced as a suture zone, respectively. In turn, the Paleoproterozoic complexes of the Tersky Terrane are thrust over the Strelna Terrane from the south.

The SGB is crosscut by the lengthy NW-trending Kolmozero–Strelna Fault, which extends in the area of our interest for a kilometer to the east from the Lesser Varzuga–Strelna interfluve (Fig. 3). The geological blocks to the east and west from the fault are distinguished by large outcrops of rocks pertaining to SGB and IVZ and by the tectonic pattern of the greenstone belt owing to various erosion levels of blocks. To the east of the Kolmozero–Strelna Fault, the configuration of the greenstone belt is rather complex: the supracrustal sequences of the Imandra Series in the form of narrow zones a few kilometers in width (maximum thickness of supracrustal rocks here is 3.5 km). The Imandra Series frames the domes composed of two-feldspar migmatites and granite, biotite and amphibole–biotite gneisses of tonalite–trondhjemite–granodiorite (TTG) association Mid-Lopian in age (~2.87 Ga) as well as of Late Lopian (2.68–2.67 Ga) alkali granite intrusions (*Gosudarstvennaya* ..., 2012). This segment of the belt is known as the Sosnovka–Strelna Domal Fold Zone.

In the Sergozero Block, to the west of Kolmozero–Strelna Fault, the morphology of SGB is substantially simplified. The total thickness of supracrustal sequences in this segment of belt reaches 14 km and larger; the strike is mainly near latitudinal, conformable to contact with IVZ. The supracrustal rocks in Sergozero Block are cut through by minor gabbro and gabbronorite bodies of the Ondomozero (1.96 Ga) and the Pyalochnozero (1.88 Ga) complexes as well as by two-feldspar pegmatoid and porphyry-like granites of the Strelna (?) Complex (~1.83 Ga) (*Gosudarstvennaya* ..., 2012).

The supracrustal rocks making up SGB are related to the Sergozero and Pyalochny Formations of the Imandra Series. The Sergozero Sequence consists of metasedimentary rocks: biotite and biotite-muscovite schists and gneisses, partly carbonaceous (protoliths corresponded to pelite, graywacke, and tuffite in composition). They are intercalated with metabasalts and metabasaltic andesites. Now they are hornblende and epidote–hornblende amphibolites and amphibole schists. Komatiitic basalts and komatiites proper have been transformed into chlorite–actinolite amphibolite and talc–chlorite–actinolite schists. To the south and the east, rocks of the Sergozero Sequence are replaced by biotite and garnet–biotite gneisses and schists of the Pyalochny Formation, which represent metasedimentary rocks with intermediate and felsic metavolcanic interlayers. They frame granite gneiss domes of basement and alkali granite intrusions (*Gosudarstvennaya* ..., 2012).

The age estimates of rocks from the Strelna Terrane and supracrustal sequences from SGB in particular are rather contradictory. The U–Pb data indicate the Upper Lopian age (2.68–2.67 Ga) of zircons from metasedimentary rocks of the Sergozero Sequence (Astaf'ev et al., 2010, 2012). Close values of rock ages at the same level of the section have been determined for orthogneiss of the Strelna Domain in the Varzuga River Valley: 2695 ± 23 and 2722 ± 18 Ma (Daly et al., 2001). Nevertheless, Sm–Nd isotopic characteristics of metasedimentary rocks and metadacites not infrequently yield Paleoproterozoic (2.06–2.45 Ga) model age (Daly et al., 2001; Timmerman and Daly, 1995). This served as a reason to represent the Strelna Terrane as a tectonic packet of Archean and Paleoproterozoic rocks (Daly et al., 2001, 2006). Taking into consideration intense metasomatic reworking of supracrustal sequences of the Strelna Belt in the Paleoproterozoic, it cannot be ruled out that Sm–Nd system of rocks are disturbed under the effect of hydrothermal fluids with the distortion of model age values. Based on isotopic U–Pb data on zircon, we suppose that rocks of the Imandra Series in SGB are Neoarchean in age.

The rocks of IVZ adjoining SGB in the north are related to the Umbian (Jatulian), Polisar (Sariolian), and Seidorechka (Sumian) suites of the Paleoprotero-

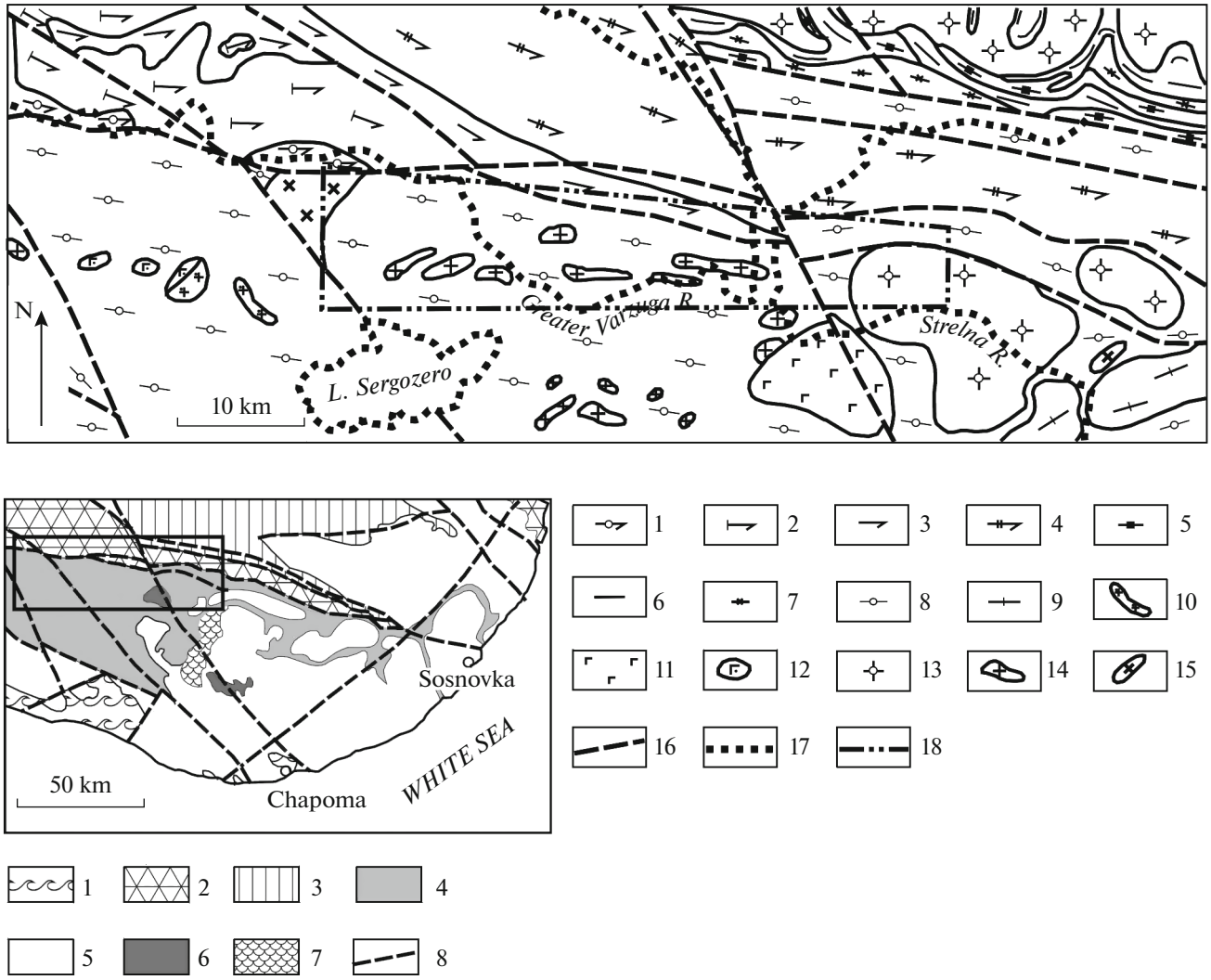

Fig. 3. Schematic geological map of eastern part of Imandra–Varzuga Zone and its framework: fragment of the State Geological Map on a scale of 1 : 1000000 (*Gosudarstvennaya* ..., 2012). (1–4) rocks of IVZ: (1) Pana Series (metamorphosed basaltic andesite, basalt, picrobasalt, mica schist partly carbonaceous); (2) Umba Formation (metamorphosed trachybasalt, tuffaceous schist, marmorized dolomite); (3) Polisar Formation (metamorphosed basalt, basaltic andesite, tuff, tuffoconglomerate); (4) Strelna Series (metamorphosed basalt, basaltic andesite, andesidacite, dacte, shale, sandstone, conglomerate); (5–7) rocks of the Minor Keivy Zone: (5) Pestsovotundra Series (plagioschist; biotite-muscovite, garnet–biotite, staurolite–biotite, and amphibole schists; arkosic sandstone, conglomerate); (6) Keivy Series (staurolite and kyanite–staurolite schists, carbonaceous schists, quartzite); (7) Ponoi Series (biotite and biotite-muscovite gneisses and schists, amphibole plagioschist, amphibolite); (8) Imandra Series of SGB (metamorphosed basalt, basaltic andesite, amphibole schist, conglomerate); (9) South Kola Complex (mainly biotite and biotite-muscovite gneisses and schists, amphibole gneiss, rare amphibolite); (10) Strelna Complex of pegmatoid granites and pegmatites (PR); (11) Pyalochnozero Complex of norite and gabbronorite (PR); (12) Ondomozero Complex of anorthosite and gabbronorite (PR); (13) Keivy Complex of alkali granites (AR); (14) migmatites and anatectic granitic complex (AR); (15) diorite–granodiorite–plagiogranite complex (AR); (16) fault; (17) the large water reservoirs; (18) boundary of the licensed area. Inset: position of Strelna greenstone complex in the schematic geological map of southeastern Kola Peninsula. (1) Neoproterozoic terrigenous complexes; (2) Paleoproterozoic volcanic–sedimentary complexes (Imandra–Varzuga and Ust-Ponoi zones; (3) Neoarchean and Paleoproterozoic Keivy volcanic–sedimentary complexes; (4) Neoarchean volcanic–sedimentary complexes of SGB; (5) Middle Lopian granite gneiss complexes of SGB; (6) norite–gabbronorite complex (PR); (7) Strelna Complex of pegmatoid granites and pegmatites; (8) main fault; rectangle is the area shown in the map (Fig. 3).

zoic. These are metamorphosed magnesian basalt, basaltic andesite, andesite, metamandelstein with amygdules filled with calcite, quartz, and epidote as well as tuff and tuffo-conglomerate.

All rocks of IVZ and SGB are metamorphosed under conditions of epidote-amphibolite or upper greenschist facies (*Imandra–Varzuga* ..., 1982; Smolkin, 1984) at the Svecofennian stage of regional metamorphism. The age of 1966 ± 13 Ma has been established with U–Pb method for metamorphic zircon from quartz–feldspar gneiss of Pyalochny Sequence (Astaf'ev et al., 2012).

In the Neoarchean complexes of SGB upthrown over Paleoproterozoic rocks of IVZ, the numerous slickensides along shears, folding of various orders, intense alteration of rocks, and development of quartz, quartz–carbonate veins and veinlets are noted. The thickness of the zone of fold–shear deformation to the south of the boundary on the side of SGB is 200–350 m. In the literature on IVZ, this zone was previously described as a "southern shear zone" (Kozlov, 1979). On the northern side of the tectonic suture, in its footwall, the rocks of IVZ are displaced and have undergone metasomatic alteration much less; the thickness of the shear zone does not exceed a few tens of meters there.

The near-boundary zone of SGB, which underwent intense fold–shear dislocations in the Paleoproterozoic, differed in high permeability for fluids and hydrothermal solutions, and this was reflected in intense development of metasomatic rocks, including mineralized ones. Astaf'ev et al. (2010) and Astaf'ev and Voinova (2010) recognize magmatogenic and metamorphic metasomatic rocks. The first were formed at the stage of greenstone belt origination in the Neoarchean and the second at the stage of its metamorphism in the Paleoproterozoic. The first are represented by garnet–muscovite and quartz–two-feldspar metasomatic rocks, which make up haloes near alkali granite. Their age (2677 ± 25 Ma) coincides with that of alkali granite. The garnet–amphibole and biotite–amphibole rocks, as well as zones of quartz veinlets and fine-grained silicification are related to products of regional metasomatism. They developed during several retrograde stages of Svecofennian metamorphism 1.86–1.77 Ga ago (Astaf'ev et al., 2010).

The classification of the considered structure as the Neoarchean greenstone belt, the metamorphic grade of supracrustal rocks corresponding to epidote-amphibolite and greenschist facies, manifestation of mafic and felsic magmatism, and widespread metasomatic rocks provide evidence for the intense reworking of rocks with fluids or solutions—all this determines a high perspective for ore deposits characteristic of greenstone belts, primarily, for gold deposits. Verification of this hypothesis was held back by, as mentioned above, difficulty of the access to the area and by its waterlogging. Nevertheless, as a result of prospecting that accompanied geological mapping carried out mainly in the 1970s–1980s by the Central Kola Expedition and the Aerogeology Scientific–Production Concern, the Vorgovy gold occurrence was discovered. The Fomkin Ruchey and Gorely Les mineralization points (Au > 1 gpt) had been revealed to the west of this occurrence as had the Olenny mineralization points in the Sosnovka–Strelna domal fold zone (Gavrilenko and Kalinin, 1997; *Gosudarstvennaya* ..., 2012). In addition, gold occurs in the amount of 5–50 signs are detected in heavy concentrates from streams. In the last edition of the State Geological Map of the Russian Federation on a scale of 1 : 1000000, the western and central parts of SGB have been pointed out as the Sergozero potential gold district.

The Central Kola Expedition performed prospecting for gold in this district in 2012–2014. The ore occurrences described in this paper have been revealed in the course of this work. Two perspective zones of chemical anomalies have been established as a result of geochemical survey. They are traced westward from the interfluve of Malaya Varzuga and Strelna rivers for more than 5 km and come abruptly eastward at the boundary of Sergozero Block (Fig. 4). Both areas of detailed works are located in the eastern part of the Sergozero Block and 2 km westward from Kolmozero–Strelna Fault. One of them is localized to the northern geochemical zone, which traces the reverse fault of Strelna Terrane over the Paleoproterozoic Imandra–Varzuga Belt. This area includes the Vorgovy ore occurrence, which was known earlier but remained poorly studied. The second area, where the Sergozero ore occurrence has been discovered as a new gold object, is located 1 km to the south from the Vorgovy occurrence within the southern anomaly zone (Fig. 4).

RESEARCH TECHNIQUE

As was said above, the main information on the studied gold ore occurrences had been obtained from results of drilling. When compiling schematic geological maps, we took the data of geochemical sampling of coarse-grained fractions of boulder piles, as well as results of magnetic survey carried out at the Sergozero ore occurrence, into consideration.

The used research technique comprises:

(1) Description of borehole cores, recognition of fold and fissility zones, and intense hydrothermal metasomatic alteration of rocks.

(2) Description of thin sections of the major varieties of metamorphic and metasomatic rocks.

(3) Fire assay with atomic absorption ending of core samples for gold at the Irkutsk Research Institute of Precious and Rare Metals and Diamonds (IRGIREDMET).

(4) ICP-OES analysis of core samples for 36 elements with decomposition in aqua-regia at IRGIREDMET, Irkutsk. The choice of this method is determined by the orientation of work to prospecting; it yields the best results for accompanying elements of gold mineralization and As, Bi, Te, Ag, Ni, Cu, Pb, S, etc.; however, incomplete recovery of such metals as Ti, Cr, W, REE, Zr, etc. does not allow us to use the obtained data for comparison of geochemical characteristics of the studied rocks with their counterparts in other geological structural units.

(5) Chemical analysis of selected samples for rock-forming elements with atomic absroption at the Chemical Laboratory of the Geological Institute,

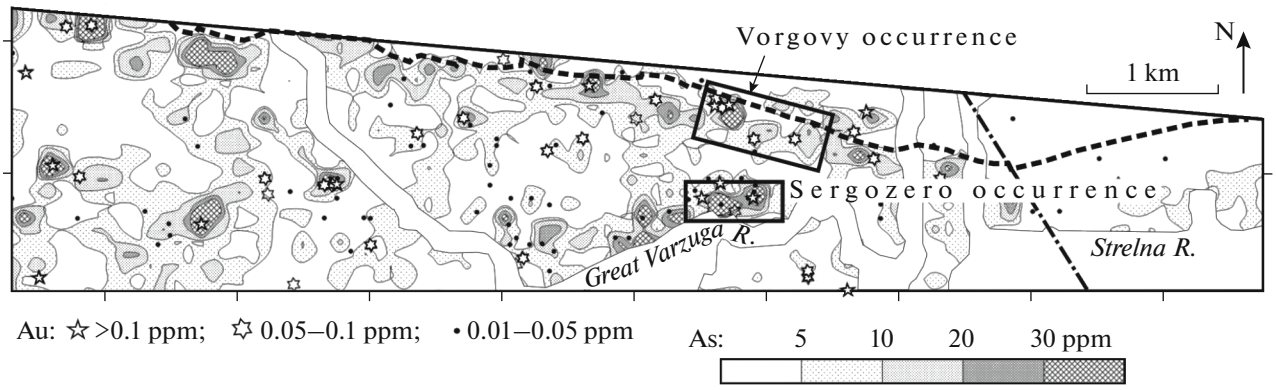

Fig. 4. Results of geochemical mapping of the Sergozero area for arsenic and gold (network of sampling is 250 × 250 m). Dashed line is the boundary of SGB and IVZ; chain line is Kolmozero–Strelna Fault.

Kola Scientific Center, Russian Academy of Sciences, Apatity.

(6) Description of polished sections of the rocks containing sulfide mineralization.

(7) Study of ore minerals with an LEO electron microscope and electron microprobe of phase composition (CAMECA MS-46, Geological Institute, Kola Scientific Center, Russian Academy of Sciences, Apatity).

(8) Selection of borehole core material for isotopic geochronological study using U–Pb and Rb–Sr methods.

The selection of zircon grains for isotopic studies was carried out using the standard technique of magnetic separation and heavy liquids. The U–Pb isotopic studies used the fractions of zircon grains various in dimensions. The internal structure of individual zircon grains was examined with an electron microscope in reflected electrons. Decomposition and chemical recovery of Pb and U was performed using the Krogh (1973) technique. A level of blank run over the period of study did not exceed 80 pg for Pb and 40 pg for U. Coordinates of points were computed in the PbDAT program (Ludwig, 1991) and ISOPLOT (Ludwig, 1999).

The isotopic compositions of Pb and U were measured on MI-1201-T and Finnigan MAT-262 (RPQ) mass-spectrometers in the static regime or with a multiplier tube. All isotope ratios have been corrected for mass-fractionation, which was acquired by study of parallel analyses of SRM-981 and SRM-982 standards, 0.18% ± 0.06% for MI-1201-T and 0.12 ± 0.04% for Finnigan MAT-262 (RPQ). The analytical uncertainties of U–Pb ratios are 0.5%. The processing of experimental data was carried out in PbDAT and ISOPLOT programs. Correction of common (unradiogenic) lead is introduced in consistence with model values (Stacey and Kramers, 1975). All uncertainties are given at a level of 2σ.

Isotopic Sr composition and Rb and Sr contents are determined on a MI-1201-T mass spectrometer in double-ribbon regime on rhenium and tantalum ribbons. The prepared samples in nitrate form are applied on ribbons. The Sr isotopic compositions in all measured samples are normalized to the value recommended by NBS in international SRM-987 standard (0.710235). Uncertainties in measured Sr isotopic composition do not exceed 0.04% (2σ) and 1.5% (2σ) for Rb/Sr ratios. The blank intralaboratory contamination with Rb is 2.5 ng and 1.2 ng with Sr.

The accepted decay constants are used in calculations of U–Pb and Rb–Sr isotope data (Steiger and Jäger, 1977).

The conditions of surveying on a MS-56 CAMECA microanalyzer are the following: accelerating voltage is 22 kV (30 kV for Re, Pb, Bi) and measure current is 30–40 nA. Synthetic compounds are used as standards (analytical lines are given in parentheses): $Fe_{10}S_{11}$ (Fe$K\alpha$, S$K\alpha$), Bi_2Se_3 (Bi$L\alpha$, Se$K\alpha$) and $LiNd(MoO_4)_2$ Mo$L\alpha$) as well as pure metals Co (Co$K\alpha$), Ni (Ni$K\alpha$), Pd (Pd$L\alpha$), Ag (Ag$L\alpha$), Te (Te$L\alpha$), Re (Re$L\alpha$), Au (Au$L\alpha$).

VORGOVY ORE OCCURRENCE

The Vorgovy ore occurrence, which is named after the creek running nearby, had been revealed in the course of geological mapping carried out by the Central Kola Expedition in the eastern part of IVZ in the mid-1980s. Owing to drilling of mapping boreholes less in diameter (nine holes 25–30 m in depth), a mineralized stockwork of quartz veins and veinlets with visible thickness (100–150 m) and no less than 1500 m in extent has been revealed (Gavrilenko, 2003; Pozhilenko et al., 2002). According to the results of fire assay, the highest gold content is 1.88 ppm.

The northern part of the mineralized area is composed of metamorphosed volcanic and sedimentary complexes of IVZ (Fig. 5). From north to south and bottom-up in the section, the members of amphibolite

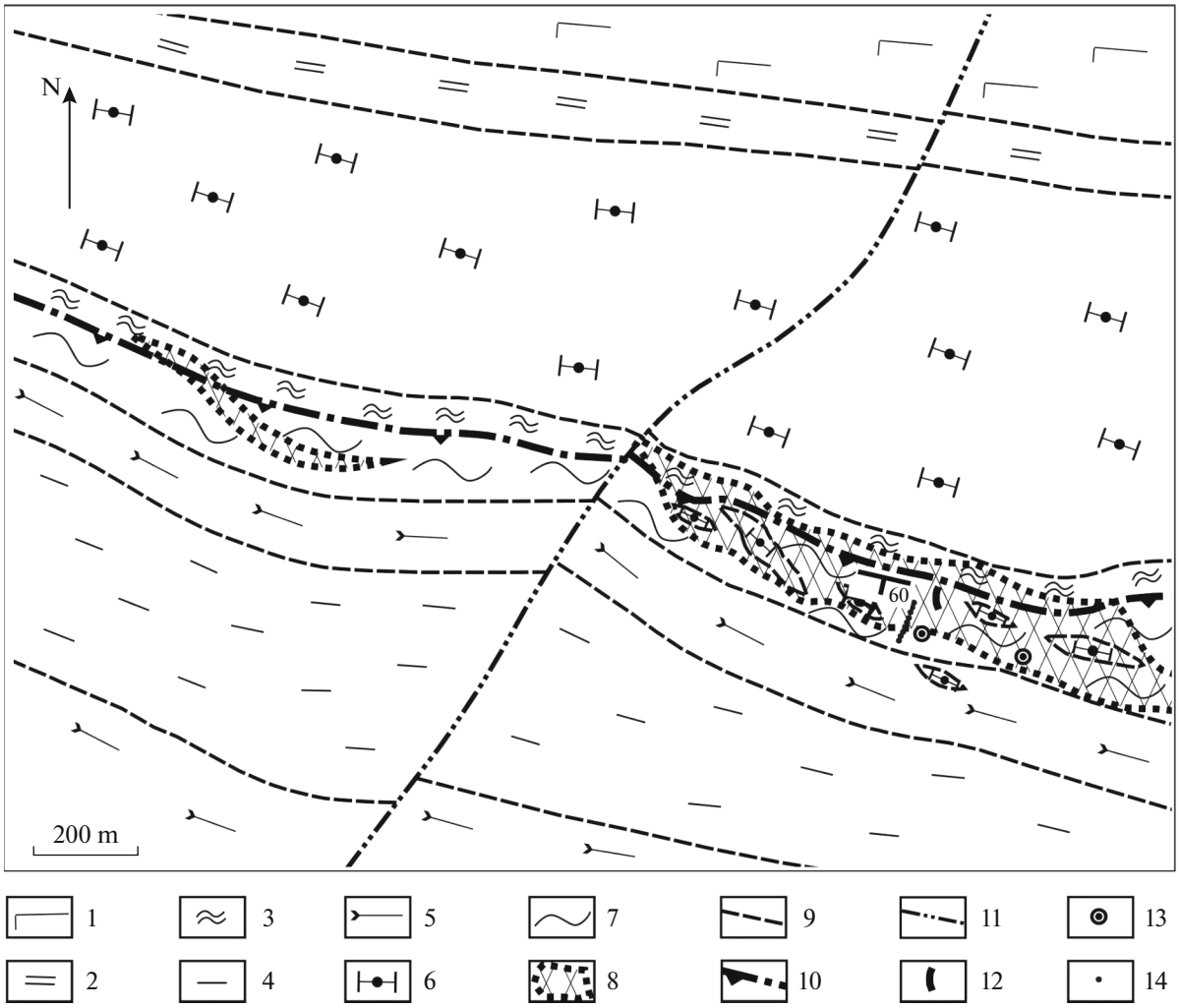

Fig. 5. Schematic geological map of Vorgovy ore occurrence. (1–3) IVZ, Seidorechka Formation: (1) amphibolite (metamandelstein), (2) biotite plagiogneiss, (3) chlorite and biotite–chlorite gneisses; (4, 5) Imandra Series of SGB: (4) biotite schist and gneiss, (5) epidote–hornblende and hornblende amphibolites; (6) chlorite–actinolite amphibolite (metaperidotite and metapyroxenite; (7) sericite–chlorite–quartz and sericite–quartz metasomatic rocks, partly graphitized; (8) stockwork of quartz and carbonate–quartz veins and veinlets; (9) supposed geological boundary, partly tectonized; (10) zone of upthrown SGB sequence over IVZ rocks; (11) late cross-cutting normal fault; (12–14) mining works: (12) trench driven by the Central Kola Expedition (CKE) in 2013, (13) borehole of CKE drilled in 2014; (14) borehole of CKE drilled in 1980.

(metamandelstein), biotite plagiogneiss (intermediate and felsic metavolcanics), and chlorite and biotite–chlorite gneisses (lavas and tuffs of meta-andesites and metabasaltic andesites) are distinguished. Such a section of volcanic rocks is characteristic of the Seidorechka Formation of IVZ. The members of biotite plagiogneisses and chlorite gneisses are divided by a massif of metaperidotite and metapyroxenite (chlorite–actinolite and talc–chlorite–actinolite amphibolites).

Intensity of hydrothermal metasomatic alteration of metavolcanic rocks from IVZ increases, approaching contact with SGB. Insignificant chloritization, less frequent biotitization, and epidotization are noted in metamandelstein. Biotite plagiogneiss is carbonated (10–25 vol % carbonate) throughout the whole mass of rock and contains separate carbonate veinlets. Chlorite gneiss is biotitized (up to 15 vol % of newly formed biotite), carbonated (10–30 vol % of carbonate), and is crosscut by abundant carbonate and carbonate–quartz veinlets. In the southern (upper) part of the chlorite gneiss member adjoining the reverse fault zone, gneisses are deformed into small folds with a wingspan of a few centimeters; the thickness of the shear zone in the gneiss is ~10 m.

The sequence of biotite schists and gneisses with interlayers of mafic and ultramafic metavolcanic rocks is upthrown over metavolcanics of IVZ at an angle of ~60°. We classified this sequence as the Sergozero Sequence of the Neoarchean Imandra Series. The biotite schists and gneisses near the reverse fault zone are intensely metasomatized and transformed into

sericite–chlorite–quartz or sericite–quartz schists at more intense alteration. A part of rocks are graphitized; nevertheless, the relict interlayers of the protolith are retained among altered rocks. The schists are deformed into folds with a limb span from a few centimeters to tens of meters; strips of delamination in zones of plication are filled with metamorphic quartz (Fig. 9a). Despite intense metasomatic transformation, two members are distinguished by mineralogy and structural features: (i) carboniferous sericite–chlorite–quartz schists and (ii) quartzite with sericite and chlorite. Rocks of different members are distinguished by grain size, content of carboniferous matter, and proportions of rock-forming minerals. This change apparently reflects initial bedding of sedimentary sequence from shale to quartz sandstone. The bodies of chlorite–actinolite amphibolites visually similar to amphibolites occurring in IVZ are identified among sericite–chlorite–quartz schists. It cannot be ruled out that this is tectonic melange.

The thickness of metasomatically altered and folded schists is approximately 150 m. Southward, the biotite schists and metasomatic rocks after them give way to the member of epidote–hornblende amphibolites (Fig. 5), then to a sequence of biotite and two-mica gneisses and schists with interlayers of various amphibolites.

Mineralization in the Vorgovy occurrence is related to a stockwork system of quartz and carbonate–quartz veins and veinlets hosted in chlorite–sericite–quartz metasomatic rocks after biotite gneiss of SGB and chlorite gneisses of IVZ (Fig. 5). The stockwork zone dips to 200° SW at an angle of 60°. The thickness of individual quartz veins and veinlets varies from a fraction of a centimeter to 2 m; stockwork zones as a whole are 100 m in thickness. The NW-trending stockwork zone extends for a minimum of 2 km and is traced down to a depth of 100 m from the surface. Quartz veinlets and lenses occur along bedding planes of conformably folded schists. The quartz content in rocks reaches 30%. The veinlets formed in two stages. The main part of veinlets is composed of early glassy coarse-grained quartz. The early sulfide phases—mainly pyrrhotite intergrown with chalcopyrite and pentlandite—are hosted in these quartz veinlets and boudins. Mineralization occurs as pockets and impregnation; the content of ore minerals is up to 3–5%. The cryptocrystalline and saccharoidal quartz of late generations occurs in selvages of veinlets and veins consisting of the early quartz or it makes up independent veinlets. The late quartz generations are coeval with carbonate and productive sulfide mineralization with native gold, including arsenopyrite, pyrite, sphalerite, and galena.

Despite the fact that the superimposed veinlets and sulfide mineralization occur within a vertical interval of ~100 m, the increased gold concentration (up to 4 ppm for 1 m in the trench and 0.6 ppm in the core of the borehole drilled for its verification) and abrupt increase in arsenic content (up to 180 ppm in the trench and up to 1000 ppm in the core of the borehole) have been established only at the contact with members composed of sericite–chlorite–quartz schist and quartzite. The formation of gold mineralization at the contact with the aforementioned members may be caused by distinct physical properties of quartz sandstone and pelite, which are favorable for filtration of Au-bearing hydrothermal solution and also for recovery of gold from solution at the reduced barrier represented by carbonaceous chlorite–sericite–quartz schists. We failed to trace gold mineralization along the strike. The borehole drilled in the same geological position 200 m to the east penetrated abundant arsenopyrite impregnations, but gold content turned out to be lower here than the detection limit of fire assay.

According to Gavrilenko (2003), gold at this ore occurrence is spongy, porous, lumpy, and not infrequently flattened in shape. Gold grains vary in size from 0.001 to 1 mm, and their predominant dimensions are 0.1–0.25 mm. Fineness of gold is 890–940‰; Cu and Fe occur as admixtures.

SERGOZERO ORE OCCURRENCE

The geological structure of the Sergozero ore occurrence is controlled by a member of mafic and ultramafic metavolcanic rocks (amphibolite, amphibole schist) 130–170 m in thickness within the sequence of fine-grained biotite–quartz and muscovite–biotite–quartz schists (Fig. 6). Interlayers of two-mica schist, partly with garnet and up to 40 m in thickness, are recorded within the member of metavolcanics as well.

The lower part of the latter member is mainly composed of chlorite–actinolite amphibolite with interlayers of talc–chlorite–actinolite schists in the lower part of the section. The protolith of chlorite–actinolite amphibolites, judging from their chemical and phase compositions, corresponds to komatiitic basalt, while talc–chlorite–actinolite schists are close to komatiite in composition (Fig. 7). It may be noted that komatiite differs from komatiitic basalt in high Mg content (magnesian numbers are 0.66 and 0.56–0.64, respectively) and in higher Cr (above 0.1% in komatiite and below this value in komatiitic basalt) along with somewhat lowered TiO_2, Al_2O_3, and alkalis contents (Table 1).

Komatiites of SGB belong to the Al-depleted type ($Al_2O_3/TiO_2 \sim 10$, $CaO/Al_2O_3 > 1$) and differ in higher Al_2O_3, TiO_2, and in relatively low iron mole fraction from komatiites of other greenstone belts in the Kola region. In these parameters, komatiite and komatiitic basalt of SGB are similar with counterparts from greenstone belts in central and eastern Karelia. In the Kola region, komatiites from the Korvatundra struc-

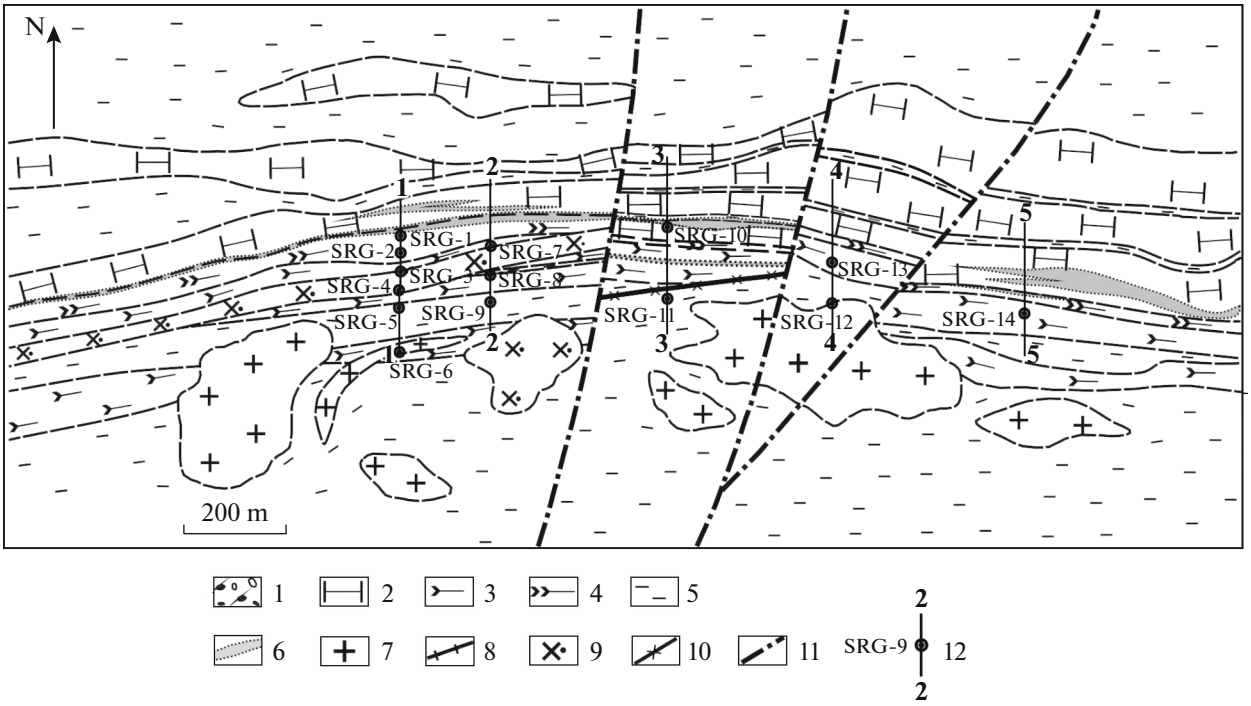

Fig. 6. Schematic geological map of Sergozero ore occurrence. Legend (also applicable to Figs. 8, 10): (1) Quaternary sediments; (2) chlorite–actinolite amphibolite (komatiitic basalt) and talc–chlortite–actinolite schist (metakomatiite); (3) hornblende and clinozoisite–hornblende amphibolite (tholeiitic basalt; (4) carbonated and silicified (banded) hornblende amphibolite; (5) muscovite–biotite–quartz and biotite–quartz plagioschists; (6) zone of intense metasomatic alteration of rocks (chlorite–calcite, biotite–calcite, biotite, quartz, and other metasomatic rocks, frequently graphite-bearing); (7) two-feldspar granite; (8) two-feldspar granitic dike, out of scale; (9) porphyritic diorite and biotite gneiss after it; (10) the same, out of scale; (11) fault; (12) line of borehole section, borehole and its number.

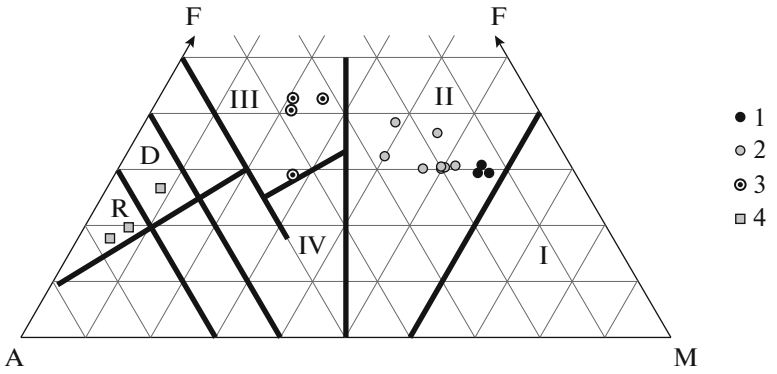

Fig. 7. AFM diagram of chemical compositon of amphibolite and porphyritic diorite of the Sergozero ore occurrence. (1) talc–chlorite–actinolite schist; (2) chlorite–actinolite amphibolite; (3) hornblende amphibolite; (4) biotite gneiss after porphyritic diorite. Fields of rock compositions (numerals in figure): I, komatiite; II, komatiitic basalt; III, tholeiitic; and IV, calc-alkaline volcanic rocks; R, rhyolite; D, dacite.

ture (Vrevsky et al., 2003) are the closest in composition.

The upper part of metavolcanic section consists of hornblende amphibolites partly with clinozoisite. They differ from chlorite–actinolite amphibolite and komatiitic basalts primarily in elevated concentrations of alkalis ($Na_2O + K_2O = 2–4$) and aluminum (alumina number is 0.61–0.80) at lowered MgO contents (magnesian number varies from 0.36 to 0.58), Cr and Ni contents (Table 2). Protolith of these rocks corresponds to tholeiitic basalt (Fig. 7).

The biotite–muscovite and biotite, partly garnet-bearing schists and gneisses, which host a member of metavolcanic rocks, are regarded as metapelites.

The supracrustal sequences are cut through by porphyritic diorite dikes up to 20 m in thickness and by

Table 1. Content of major (wt %) and minor elements (ppm) in komatiites and komatiitic basalts from Sergozero occurrence

Sample No.	011300	010294	011578	011450	011435	011561	011554	011535	011446	011543	011551
SiO_2	41.59	39.38	41.13	43.64	43.73	42.62	44.52	45.21	42.66	43.70	44.03
TiO_2	0.60	0.59	0.65	0.81	1.16	0.90	1.03	0.91	0.84	0.92	0.83
Al_2O_3	5.04	4.61	5.95	6.74	6.88	9.32	8.69	10.10	7.24	7.75	7.73
Fe_2O_3	4.93	4.20	4.63	1.99	6.74	2.67	7.30	2.70	3.81	4.17	4.04
FeO	6.16	6.19	6.88	9.18	6.94	8.99	6.90	8.50	6.64	7.48	7.23
MnO	0.15	0.17	0.17	0.16	0.17	0.18	0.15	0.17	0.19	0.19	0.18
MgO	21.71	18.92	21.88	19.61	17.70	18.91	14.30	14.37	17.81	19.81	18.97
CaO	7.39	10.48	8.30	9.93	7.58	8.56	6.68	9.23	8.62	8.81	9.27
Na_2O	0.04	0.04	0.11	0.71	0.24	0.59	1.19	1.87	0.65	0.48	0.39
K_2O	0.01	0.23	0.05	0.50	0.52	0.22	1.14	0.54	0.91	0.22	1.35
H_2O^-	0.28	0.29	0.20	0.21	0.23	0.28	0.21	0.23	0.39	0.28	0.25
LOI	5.77	6.27	5.55	4.37	4.18	5.07	3.54	3.76	3.09	4.40	3.71
Li_2O	0.0033	0.0035	0.0019	0.0052	0.0051	0.0061	0.0061	0.0048	0.0066	0.0057	0.0068
Rb_2O	0.0007	0.0011	0.0006	0.0016	0.0019	0.0007	0.0034	0.0019	0.0025	0.0009	0.0038
Cs_2O	0.00013	0.00019	0.00010	0.00026	0.00015	0.00000	0.00027	0.00020	0.00025	0.00009	0.00028
P_2O_5	0.06	0.06	0.05	0.08	0.13	0.08	0.14	0.09	0.04	0.08	0.06
S_{tot}	0.17	0.21	0.23	0.09	2.41	0.05	2.62	0.16	1.00	0.51	0.42
CO_2	6.45	8.62	3.80	2.45	1.81	1.38	1.15	2.65	5.73	1.28	1.71
Total	100.35	100.26	99.58	100.48	100.43	99.83	99.57	100.50	99.63	100.09	100.18
FeO*	10.60	9.97	11.05	10.97	13.01	11.39	13.47	10.93	10.07	11.23	10.87
$Na_2O + K_2O$	0.05	0.27	0.16	1.21	0.76	0.81	2.33	2.41	1.56	0.70	1.74
mg'	0.66	0.65	0.66	0.64	0.56	0.62	0.50	0.56	0.63	0.63	0.63
al'	0.15	0.16	0.18	0.22	0.22	0.30	0.30	0.39	0.26	0.25	0.26
Al_2O_3/TiO_2	8.40	7.81	9.15	8.32	5.93	10.36	8.44	11.10	8.62	8.42	9.31
CaO/Al_2O_3	1.47	2.27	1.39	1.47	1.10	0.92	0.77	0.91	1.19	1.14	1.20
Au	0.003	0.005	0.003	0.003	0.010	0.012	0.059	0.008	2.710	5.300	1.505
As	9	23	24	71	2	59	78	17	1405	534	1223
Cu	74	167	88	79	164	66	246	127	86	78	53
Ni	449	440	490	435	516	258	589	220	494	614	573
Co	41	46	44	48	54	35	65	35	56	79	66
Cr	1064	1056	1081	786	719	556	719	499	1003	847	886
V	110	122	94	74	125	68	142	107	149	82	108
Pb	2	2	9	12	17	2	2	2	33	2	2
Zn	36	37	31	38	130	28	112	36	83	40	46
Ba	3	23	3	69	111	30	172	101	111	18	190
Sr	73	105	34	186	87	41	35	90	252	33	78
P	171	167	167	248	556	234	498	274	73	259	114
La	2	2	2	2	14	2	11	2	4	2	2
Y	3.7	5.4	3.1	1.5	3.8	1.5	4.5	3.2	5.1	1.5	1.5
Zr	1.0	1.0	1.0	1.0	19.6	1.0	23.6	1.0	3.0	1.0	1.0

Rock samples: 011300, talc–chlorite–actinolite schist; 010294, talc–chlorite–carbonate rock; 011578, actinolite–chlorite schist; 011450, 011435, 011543, chlorite–actinolite schist; 011446, 011551, the same, biotitized; 011561, 011535, actinolitic amphibolite; 011554, actinolitic amphibolite biotitized. Magnesian and alumina numbers and element ratios have been calculated after exclusion of H_2O^-, LOI, CO_2 and recalculation of rock composition for 100%.

Table 2. Content of major (wt %) and minor elements (ppm) in hornblende amphibolite and porphyritic diorite from Sergozero occurrence

Sample No.	007774	011353	011478	011428	011028	011396	011390
SiO_2	47.74	48.89	47.06	45.61	57.85	59.62	67.21
TiO_2	0.55	1.35	1.08	2.49	0.61	0.72	0.30
Al_2O_3	13.70	12.46	12.74	12.19	19.27	17.18	15.78
Fe_2O_3	1.17	2.60	3.31	2.17	1.31	2.06	1.84
FeO	7.58	10.76	9.63	11.68	3.42	4.47	1.73
MnO	0.16	0.21	0.20	0.19	0.07	0.10	0.06
MgO	8.47	6.94	7.06	9.39	1.73	2.05	0.96
CaO	11.92	10.92	8.99	7.93	4.87	5.60	3.40
Na_2O	2.75	2.37	3.18	2.67	5.35	3.71	3.57
K_2O	0.33	0.33	0.64	0.93	1.81	1.92	2.45
H_2O^-	0.00	0.20	0.35	0.16	0.00	0.04	0.05
LOI	2.22	1.51	3.09	3.17	0.70	0.87	0.42
Li_2O	0.0043	0.0029	0.0045	0.0055	0.0053	0.0054	0.0039
Rb_2O	0.0012	0.0014	0.0021	0.0025	0.01	0.0078	0.0074
Cs_2O	0.00009	0.00018	0.00013	0.00026	0.00016	0.00018	0.00022
P_2O_5	0.04	0.12	0.14	0.24	0.16	0.23	0.13
S_{tot}	0.02	0.14	0.05	0.07	0.86	0.15	0.54
CO_2	2.89	1.38	2.56	1.35	1.17	0.78	1.28
Total	99.55	100.18	100.09	100.25	99.19	99.51	99.73
FeO*	8.63	13.10	12.61	13.63	4.599	6.32	3.39
$Na_2O + K_2O$	3.08	2.70	3.82	3.60	7.16	5.63	6.02
mg'	0.49	0.34	0.35	0.40	0.27	0.24	0.21
al'	0.80	0.61	0.64	0.52	2.98	2.00	3.48
Au	0.016	0.003	0.036	0.015	0.030	0.005	0.130
As	37	2	60	65	19	33	201
Cu	64	72	67	35	44	13	22
Ni	35	21	22	86	5	6	5
Co	20	19	49	39	6	12	5
Cr	65	42	60	168	56	69	73
V	31	63	141	159	8	23	3
Pb	2	2	2	2	57	13	28
Zn	19	25	52	91	122	85	52
Ba	3	3	38	323	159	621	188
Sr	14	10	19	36	36	29	30
P	195	447	558	1021	681	896	487
La	2	2	2	24	46	40	36
Y	1.5	6.3	7.9	5.3	7	4.6	5.5
Zr	1.0	3.0	1.0	8.2	23	22.2	30.4

Rock samples: 007774, 011353, and 011478, hornblende amphibolite biotitized to a various degree; 011428, chlorite–biotite schist after hornblende amphibolite; 011028 and 011396, biotite gneiss after porphyritic diorite; 011390, the same, intensely silicified.

minor intrusions of porphyry-like minor bodies. Dikes of porphyritic diorite crosscut the host amphibolites and biotite-muscovite gneisses at an acute angle (Figs. 6, 8); contacts of dikes are sharp, uneven, or sinuous. Porphyritic diorite is foliated but retains primary porphyry texture (Fig. 9c). The fine-grained biotite–quartz–plagioclase matrix contains oligoclase phenocrysts up to 1.5 mm in size. Their shape is rounded or irregular and occasionally emphasized by secondary alteration of mineral (Fig. 9c). According to the classification by Jensen (1976), the chemical composition of biotite gneiss after porphyritic diorite corresponds to rhyolite and dacite of the tholeiitic series (Fig. 7). The $Na_2O + K_2O$ sum ranges from 5.8 to 7.4 wt % and sodium is prevalent over potassium (Na_2O/K_2O = 1.5–2.8). The alumina and silica contents are 16–20 and ~60 wt %, respectively, up to 70% in silicified varieties (Table 2).

A series of minor granite bodies is localized in the southern part of the area, where they are hosted in a sequence of mica–quartz plagioschists overlying the amphibolite member (Fig. 6). The granitic bodies are oval in shape with the long axis oriented according to the strike of host rocks, occupying an area of 0.3 × 0.6 km. In addition, the boreholes penetrate the crosscutting veins from a few centimeters to 9 m in thickness. Granites are porphyry-like; the large feldspar grains (up to 3–4 mm in microcline varieties and up to 1.5 mm in plagiogranite) are incorporated into a fine-grained muscovite–feldspar–quartz matrix. The feldspar contents are variable: from quartz–microcline rocks with 70% of microcline to plagiogranite with 55% oligoclase. Two-feldspar granites are the youngest pre-Quaternary rocks in the studied territory. They are apparently related to the Strelna Complex of pegmatoid granite ~1.83 Ga in age (*Gosudarstvennaya ...*, 2012).

All rocks of the Sergozero area are foliated, deformed into small folds, broken by a network of late veinlets, are brecciated locally (viscous flow is combined with brittle failure), and metasomatically altered. The most intense ductile deformation and metasomatic transformation are related to fault zones conformable to the attitude of rocks and foliation. Such zones are marked by gray color in Figs. 6, 8, and 10. The main metasomatic alterations of rocks are represented by chloritization (up to 60 vol % newly formed chlorite), biotitization (up to 10% biotite in rock), carbonation, graphitization, and silicification. The above-mentioned secondary processes are generally listed in order of their superposition, although, for example, not less than two stages of chloritization may be recognized (before and after crystallization of biotite). In the rocks enriched in plagioclase (hornblende amphibolite, porphyritic diorite), epidotization and related crystallization of titanite predate the aforementioned processes. The total thickness of the tract characterized by relatively intense metasomatic alteration of rocks is 60–120 m, approximately 80 m on average (Figs. 8, 10). This tract comprises the entire sequence of hornblende amphibolites, the upper part of the chlorite–actinolite rocks, and porphyritic diorite dikes crosscutting amphibolite. The areas of metasomatic transformation differing in degree of intensity are contoured within the tract; the share of newly formed minerals may exceed 50% of rock volume.

In the case of biotitization, amphiboles—hornblende or actinolite—are replaced in the first place (Fig. 9d). Biotite develops mainly as strips up to 2 mm in thickness, which are concordant to foliation. Therefore, biotitized amphibolites are frequently banded. Magnesium number (Mg/(Mg + Fe)) of superimposed biotite is variable (0.59–0.74). Depending on intensity of biotitization, potassium content in amphibolite changes, reaching 1.4%, and this is reflected in various K/Na ratios. The Rb and Ba contents change proportionally to potassium (Tables 1, 2).

The early superimposed chlorite also replaces mainly hornblende, whereas the late chlorite develops after both amphibole and biotite; chloritization of amphibolite increases MgO content in the latter (Table 2).

Calcite crystallizes in parallel with biotitization and early chloritization (the share of calcite end-member in carbonate is 97–98%) in form of xenomorphic grains somewhat larger than the grains of the silicate matrix. As a result, biotite–calcite and chlorite–calcite metasomatic rocks are formed. The latter occur mainly in the hornblende amphibolite sequence in the upper part of the zones characterized by intense metasomatic alteration, whereas the former gravitates to its lower part, where hornblende and chlorite–actinolite amphibolites serve as protoliths as does porphyritic diorite of the dike complex. The outlined zoning of metasomatic transformation may be related to both chemical and thermal causes: the biotite–calcite metasomatic rocks are higher-temperature than chlorite–calcite (Kol'tsov, 1996). The chlorite–calcite and biotite–calcite metasomatic rocks developed against the background of viscous deformations. Plication with the span of fold limbs measured a few centimeters.

Silicification results in formation of metasomatic quartzite. This is a banded rock, where fine- and medium-grained bands intercalating with thin relict interbeds of fine-grained protoliths: hornblende or chlorite–actinolite amphibolites, gneissose porphyritic diorite, two-mica gneisses, and schists. In time, this process is later than the formation of biotite–calcite and chlorite–calcite metasomatic rocks. Silicification develops more intensely in biotite and two-mica gneisses and schists as well as in hornblende amphibolite rather than in chlorite–actinolite amphibolite and schists formed after them. Boundaries between quartzite and other rocks are crosscutting; the

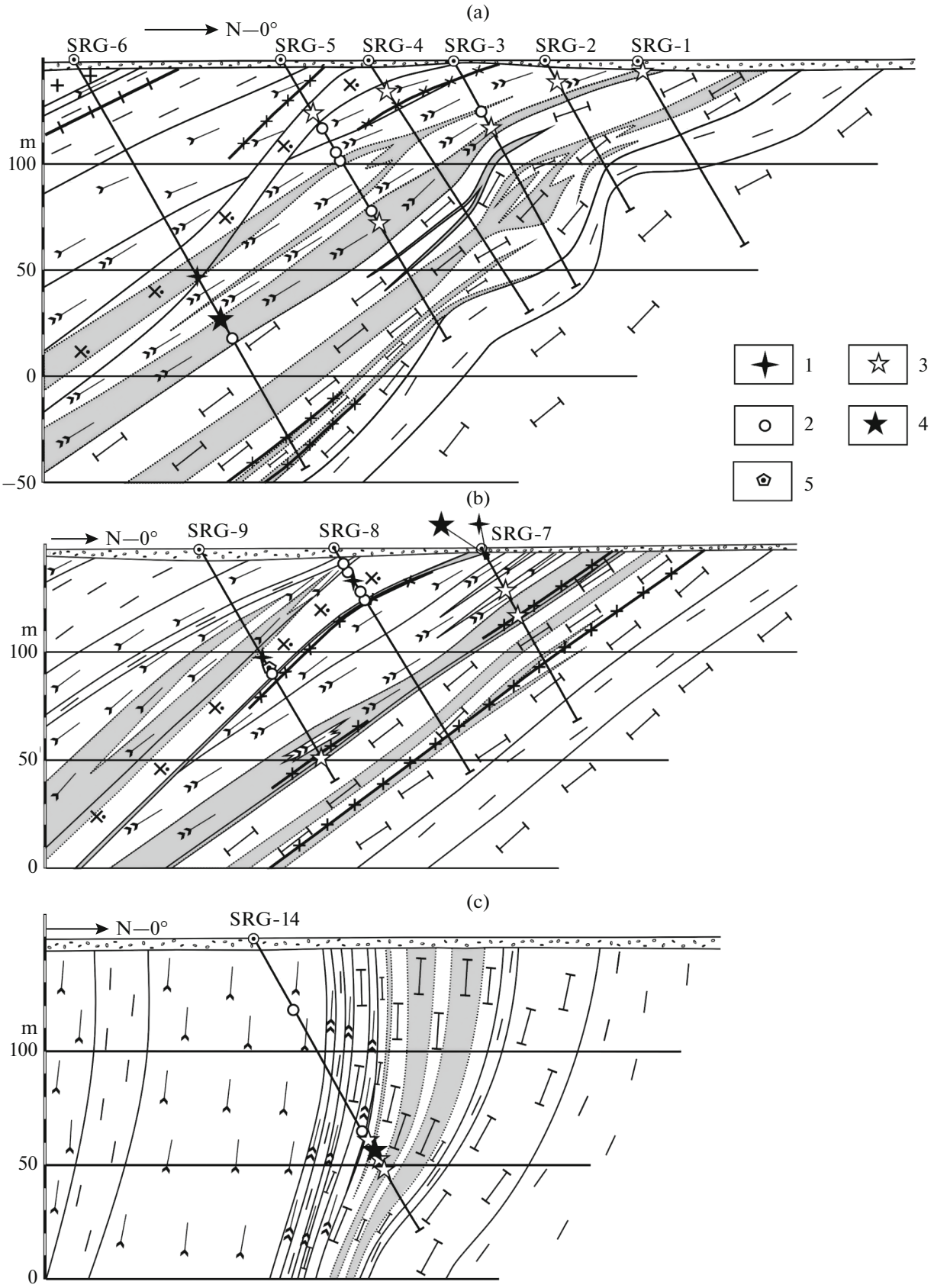

Fig. 8. Geological sections of Sergozero ore occurrence: (a) profile 1–1; (b) profile 2–2, (c) profile 5–5. (1) Bismuth mineralization; (2–4) gold contents in samples: (2) 0.5–1.0 ppm, (3) 1–5 ppm, (4) >5 ppm; (5) location of samples assigned for geochronological study. See Fig. 6 for other symbols.

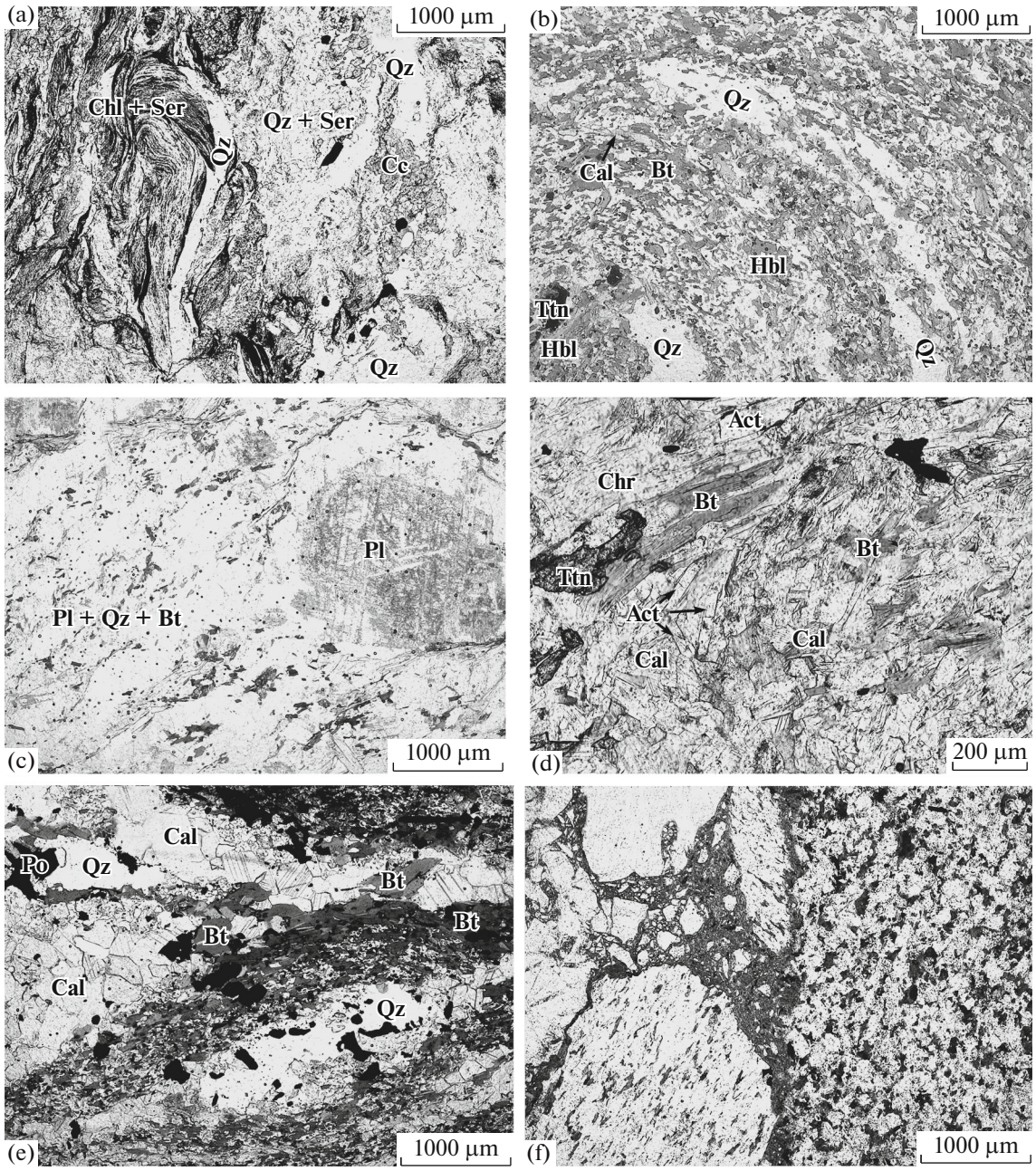

Fig. 9. Rocks from (a) Vorgovy and (b–f) Sergozero ore occurrences. Transmitted light, crossed polars. (a) Chlorite–sericite–quartz metasomatic rock with quartz venlets saturated with carbonaceous matter, Vorgovy ore occurrence; (b) folds in silicified and biotitized hornblende amphibolite; (c) zonal plagioclase phenocrysts in porphyritic diorite; (d) formation of calcite and biotite after chlorite–actinolite amphibolite; (e) calcite–biotite metasomatic rock after hornblende amphibolite; black rash in biotite is carbonaceous matter; the Au content in rock is 5.7 ppm for 1.1 m; (f) brecciated biotite plagiogneiss: various orientation of foliation in fragments is seen. Act, actinolite; Bt, biotite; Cal, calcite; Chl, chlorite; Hbl, hornblende; Pl plagioclase; Po, pyrrhotite; Qz, quartz; Ser, sericite; Ttn, titanite.

sinuous shape of quartzite bodies is irregular. Intense silicification is accompanied by the formation of quartz and carbonate–quartz veinlets, which frequently occupy more than 10 vol % of rock and mainly develop conformably to foliation, imparting a characteristic banded appearance (transition to brittle failure). Recrystallization and redeposition of pyrrhotite and arsenopyrte are first related to quartz and carbonate–quartz veins and are followed by the formation of superimposed galena–arsenopyrite mineralization in porphyritic diorite replaced with quartz.

Graphitization is recorded in all rocks, except for granitic dikes, as bands (zones) up to tens of meters in thickness (Fig. 8), which intersect stratigraphic

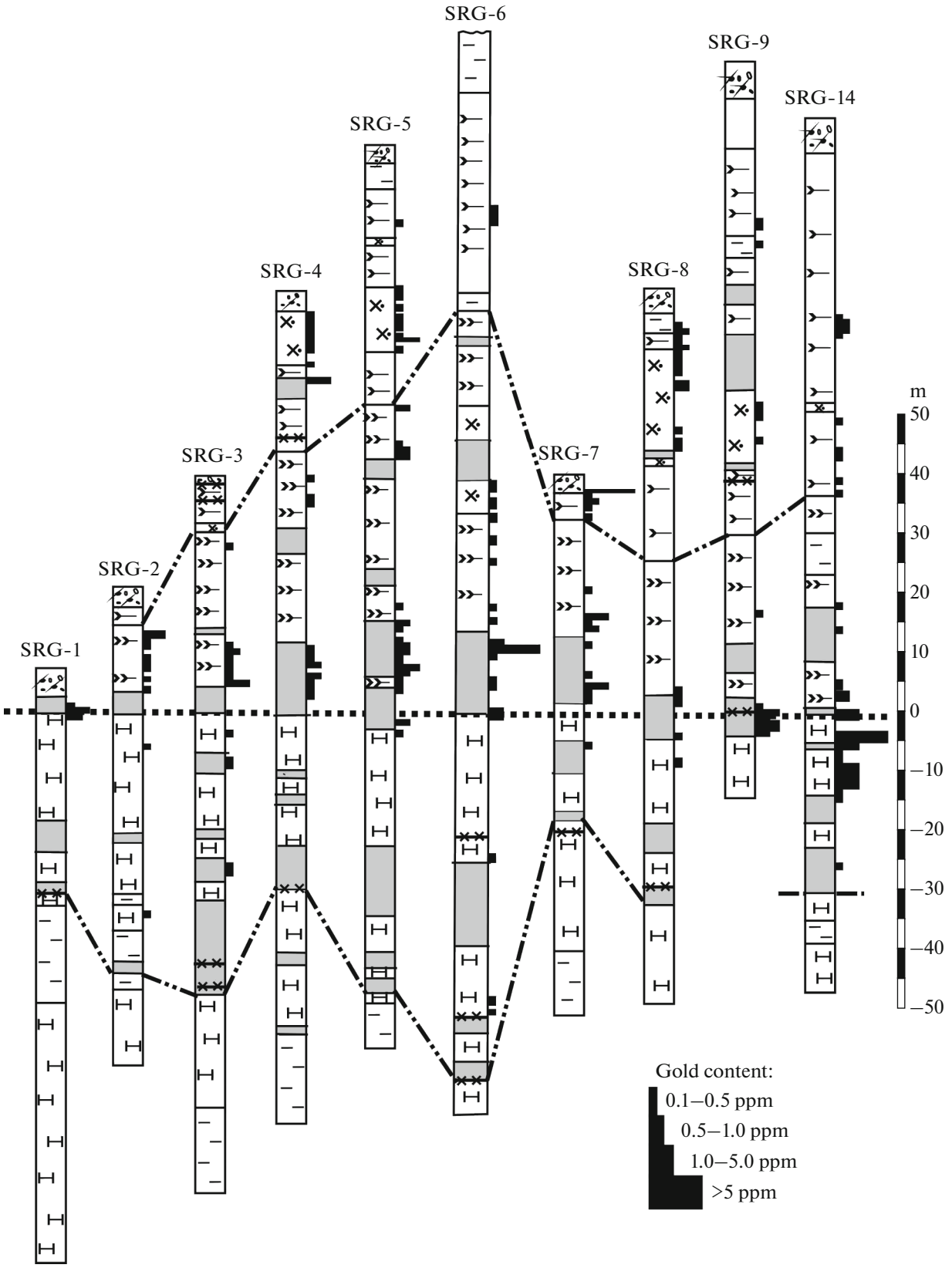

Fig. 10. Position of samples with elevated gold content relative to zone of metasomatic alteration of rock (chain line) and contact of hornblende and chlorite amphibolite metasomatic rock (dotted line). See Fig. 6 for legend.

boundaries. The zones of graphitization coincide, to a certain measure, with zones of intense metasomatic transformation and record the channels for migration of metasomatic solutions/fluids. One of such zones is related to the contact between hornblende and chlorite–actinolite metasomatic rocks, affecting not only aforementioned amphibolites but also biotite and biotite-muscovite gneisses and dikes of porphyritic diorite. A concentration of carbonaceous matter may reach several percent. In thin sections, distribution of carbonaceous matter (graphite) is always nonuniform, such as bands parallel to foliation, "streams" crosscutting foliation at an acute angle, or as superimposed spots (Fig. 9f). Graphitization is recorded only in carbonated rocks, although it may be related to various minerals in rock graphite—calcite, biotite, actinolite, chlorite, muscovite, etc.—and no rules in its distribution are revealed. The subsequent, later than graphitization, superimposed processes give rise to redistribution of carbonaceous matter. Thus, exocontact zones of conformable and crosscutting quartz–carbonate veinlets are quite often enriched in carbonaceous matter.

Zones of brecciation have been opened by boreholes in biotite-muscovite gneisses (metapelites) at various levels of section both lower and higher than member of amphibolites and in porphyritic diorite dikes (biotite gneiss) that cut through amphibolite. A breccia-like structure has also been established in amphibolite broken by a dense network of chlorite and/or carbonate veinlets. The visible thickness of breccia in boreholes is less than 3 m; we failed to establish elements of its attitude and to coordinate zones of brecciation in borehole sections. In breccia, the fragments of gneiss are irregular in shape and a few centimeters in size; they are often angular and cemented with fine-grained gangue material consisting of carbonate, chlorite, epidote, and quartz. The fragments occupy 80–90 vol % of rock. The larger voids are filled with late quartz characterized by structures of mineral growth typical of fracture filling or with calcite. The formation of breccia is caused by multifold development of hydrothermal veinlets; this is corroborated by an increase in number of hydrothermal veinlets in host rocks with the approaching zone of brecciation. At the same time, the role of late tectonics is doubtless: variable direction of schistosity in neighboring gneiss fragments within one sample is evidence (Fig. 9f).

The Sergozero occurrence is broken into three blocks by steeply dipping normal faults striking in near-meridional and northeastern directions. The tectonic blocks are recognized by the interpretation of magnetometric data owing to the abrupt disappearance and displacement of relatively magnetic rock members. The results of borehole drilling revealed distinctions in the geological structure of blocks. In the western block, where borehole profiles 1–1 and 2–2 have been drilled, rocks dip at an angle of 30° in southern bearings (Figs. 8a, 8b). The thickness of amphibolite sequence is approximately 140 m. In addition, porphyritic diorite dikes up to 20 m in thickness are rather widespread in the western block. In the eastern block (profile 5–5), dip angle of rocks increases up to steep (65°–75°) (Fig. 8c). The thickness of amphibolite member increases here up to ~400 m. The porphyritic diorite dikes in the eastern block are rare and thin (<1 m). In the central block, which has the shape of a wedge widening to the north, all parameters are intermediate between values established for the western and the eastern blocks. The blocks of this ore occurrence differ in intensity of metasomatic transformation. A maximum of intensity is established in the central block and a minimum in the eastern block.

Sulfide mineralization is characteristic of all rocks of ore occurrence with the exception of two-feldspar granite. The content of ore minerals and chemical composition of mineralization depend on the type of host rock and the character and intensity of superimposed processes. Three types of mineralization are recognized with confidence:

(1) The early background mineralization of massive-sulfide type substantially pyrrhotite in composition (pyrrhotite with ingrowths chalcopyrite, sphalerite, and flame-like pentlandite) in all rocks of ore occurrence both weakly and intensely altered. Structure of mineralization is disseminated; sulfide contents in two-mica and biotite gneisses are up to 1 and 3% in amphibolite. In quartz–carbonate veinlet lodes, the content of ore minerals increases up to 10–15%; the structure of mineralization is characterized by pockets and veinlets.

(2) The superimposed arsenopyrite mineralization, which is controlled by zones of hydrothermal metasomatic alteration of hornblende and chlorite–actinolite amphibolites and porphyritic diorite. In addition to arsenopyrite, this mineralization contains pyrite, gersdorffite, pentlandite, galena, molybdenite, scheelite, native gold; sporadic ullmannite NiSbS and hessite Ag_2Te are identified. Metasomatic rocks after chlorite–actinolite amphibolite are markedly enriched in Ni minerals—pentlandite and gersdorffite—up to predominance of the latter over arsenopyrite. Structure of mineralization is disseminated, stringer–disseminated, with rare pockets; the content of ore mineral is up to 10%.

(3) Arsenopyrite–galena with bismuth in zones of silicification and brecciation of porphyritic diorite (Fig. 8). Sulfides—galena, arsenopyrite, pyrrhotite, sphalerite—make up disseminations and microstringers along boundaries of quartz grains; the content of ore minerals reaches 3%; grain size is up to 1 mm. Native bismuth and other Bi-bearing minerals (bismoclite BiOCl, hedleyite Bi_7Te_3, ikunolite $Bi_4(S,Se)_3$, as well as silver phases (matildite $AgBiS_2$, proustite Ag_3AsS_3), and Ag–Bi–S, Au–Bi–Fe–Ag–S, Ag–As–S, Ag–Fe–S compounds with proportions of elements that do not correspond to formulae of known

mineral phases occur as inclusions in marginal parts of galena grains or within fractures in quartz nearby large galena grains. Dimensions of native bismuth segregations are up to 50 μm, and other bismuth phases are smaller than 5 μm.

The main stage of gold formation is related to origination of arsenopyrite and gersdorffite. The link between gold and bismuth mineralization is outlined: the samples with high bismuth content (29–92 ppm) are enriched in Au (0.7–17 ppm); however, the scale of bismuth mineralization in the object is quite insignificant, so that the available data on estimation of this relationship are currently insufficient.

The zone of second-stage arsenopyrite mineralization coincides with the afore-described zone of intense metasomatic transformation of rocks approximately 80 m in thickness, i.e., it embraces the lower part (more than half in thickness) of hornblende-amphibolite sequence and the upper part of chlorite–actinolite amphibolite sequence. Arsenopyrite makes up here impregnations of hypidiomorphic and idiomorphic grains of rhombic habitus; their size reaches 1 mm. Distribution of the mineral is not uniform; lenses are up to few meters in thickness. In the boreholes penetrating the zone of intense metasomatic transformation, the intervals with As content higher than 100 ppm make up less than 30% of its thickness and much lesser with visible arsenopyrite, which frequently replaces early sulfides (pyrrotite, chalcopyrite). Its intergrowths with other minerals are relatively rare. Most often these are galena micrograins at the boundary with gangue minerals or grains of late pyrite. In rare cases of arsenopyrite individuals from disseminated mineralization, zoning is revealed: the inner zone is enriched in arsenic and the outer zone is close to As : S = 1 : 1 (Table 3).

During formation of carbonate–quartz and quartz veinlets, arsenopyrite is recrystallized, forming metacrystals up to 5 and occasionally 8 mm in size with numerous inclusions of pyrrhotite, chalcopyrite, and less abundant galena and sphalerite as well as ilmenite and native gold. Arsenopyrite metacrystals commonly occur in marginal parts of veinlets and their exocontact zones rather than within veinlets. Metacrystals display zonal distribution of As/S ratio more frequently than in arsenopyrite individuals of disseminated mineralization. This zoning is readily discernible under a microscope.

Arsenopyrite is characterized by minor Ni admixtures (up to 2%) and Co (up to 1.75%) along with a certain excess of As in respect to S (Table 3). The As content (34.5–35.4 at %) in arsenopyrite in association with pyrrhotite (without pyrite) indicates that ore was formed at a temperature of 480–550°C (Kretschmar and Scott, 1976; Bortnikov et al., 1993) in consistence with the temperature of host rocks' metamorphism.

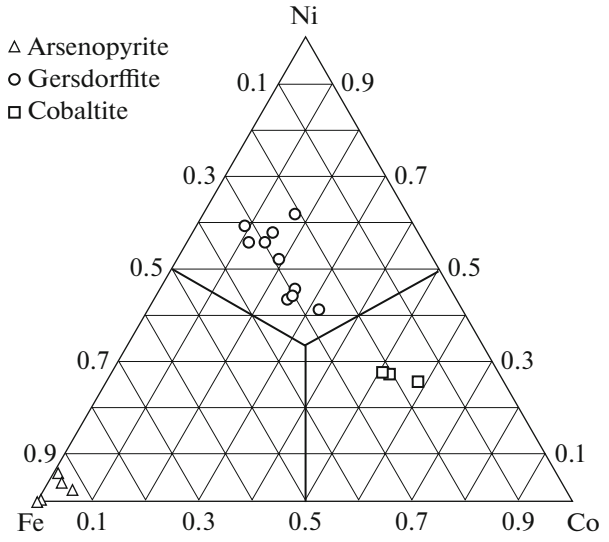

Fig. 11. Diagram of Fe, Ni, and Co sulfoarsenides.

Minerals of the gersdorffite–cobaltite series have been identified only in metasomatic rocks after chlorite–actinolite schists and amphibolites. In particular cases, precisely gersdorffite becomes the major mineral in rock. The hypidiomorphic up to idiomorphic cubic gersdorffite grains are up to 0.3 mm in size. Gersdorffite replaces pyrrhotite as sheath crystals. In addition to pyrrhotite, the intergrowths with gersdorffite are noted for arsenopyrite, pentlandite, and galena. The latter mineral occurs as microsegregations along fractures in gersdorffite, and, together with ullmannite, develops at the boundary of gersdorffite with gangue minerals. The composition of gersdorffite is characterized by variable Ni : Co : Fe ratio up to predominant of cobaltite end member (Table 3; Fig. 11).

The high gold contents from 1 to 5.7 gpt are related to the boundary between hornblende and chlorite–actinolite amphibolites in the main ore zone (Fig. 10). In section 1–1 of the western block, the gold mineralization (3.3 gpt for 2.2 m in Hole SRG-6) is recorded at the bottom of hornblende amphibolite. In section 2–2 of the western block at the contact of two amphibolite sequences, the dike of porphyritic diorite is localized. The gold mineralization (1.95 gpt for 4.3 m in Hole SRG-9) is recorded in both porphyritic diorite of the western block and the upper part of chlorite–actinolite amphibolite. In the eastern block (section 5–5), gold (2.13 gpt for thickness of 13.7 m in Hole SRG-14) is related to the upper part of the chlorite–actinolite amphibolite sequence (Fig. 10). In all three cases, the high gold contents are confined to well-expressed biotite–calcite metasomatic rocks developing after hornblende amphibolite, porphyritic diorite, and chlorite–actinolite amphibolite.

Upsection, in the zone of arsenopyrite mineralization, the gold content in altered hornblende amphibolite

Table 3. Chemical composition (wt %) of sulfoarsenides and native gold from the Sergozero occurrence (microprobe data)

Chemical element	SRG-6-141.0	K-12-61.0	SRG114-113.4	SRG-8-8.7	SRG-8-17.3	SRG2*	SRG2*	SRG2*	SRG2*
	1	2	3	4	5	6	7	8	9
Fe	33.67	30.94	30.84	32.55	33.93	30.95	34.11	33.59	33.99
Co	0	0.21	0.82	0.17	0	1.76	n.a.	n.a.	n.a.
Ni	0.03	2.09	1.37	0.13	0	0.85	n.a.	n.a.	n.a.
Cu	0	0	0	0	0	n.a.	n.a.	n.a.	n.a.
Ag	0	n.a.	0	0	0.11	n.a.	n.a.	n.a.	n.a.
Au	0	0	0	0	0	n.a.	n.a.	n.a.	n.a.
Hg	0	n.a.	n.a.	n.a.	n.a.	n.a.	n.a.	n.a.	n.a.
As	47.35	48.87	47.85	47.86	47.21	49.34	46.83	48.96	46.29
Sb	0.11	0.09	0	0	0	n.a.	n.a.	n.a.	n.a.
S	18.78	17.36	18.29	18.41	18.75	17.10	19.06	17.45	19.72
Total	99.94	99.56	99.17	99.12	99.99	100	100	100	100
Coefficients of crystal chemical formula									
Fe	0.990	0.928	0.914	0.961	1.000	0.929	1.001	1.003	0.991
Co	0.000	0.006	0.023	0.005	0.000	0.024			
Ni	0.001	0.060	0.039	0.004	0.000	0.050			
Cu	0.000	0.000	0.000	0.000	0.000				
Ag	0.000		0.000	0.000	0.002				
Au	0.000	0.000	0.000	0.000	0.000				
Hg	0.000								
As	1.037	1.092	1.056	1.053	1.037	1.103	1.025	1.09	1.007
Sb	0.001	0.001	0.000	0.000	0.000				
S	0.961	0.907	0.944	0.947	0.963	0.894	0.974	0.908	1.002

Table 3. (Contd.)

Chemical element	СРГ14-113.4	СРГ14-109.8	СРГ14-109.8	СРГ-3-24.7	СРГ14-109.7	СРГ14-109.8	СРГ14-113.4	СРГ-6-141.0	СРГ-6-141.0	СРГ-6-141.0	СРГ-8-8.7
	10	11	12	13	14*	15*	16	17	18*	19*	20
Fe	11.12	10.06	7.14	5.65	0.79	n.a.	0.17	0.15	0.55	0.72	0.16
Co	3.1	8.73	5.83	20.2	n.a.	n.a.	0	0.02	n.a.	n.a.	0
Ni	20.81	15.94	20.92	8.98	n.a.	n.a.	0.054	0	0.20	n.a.	0
Cu	0	0	0.14	0	0.82	n.a.	0	0	n.a.	n.a.	0
Ag	0	0	0	0	31.23	14.24	14.96	3.57	5.35	6.07	30.62
Au	0	0	0	0	67.16	85.76	83.31	95.83	93.90	93.22	65.48
Hg	n.a.	n.a.	n.a.	n.a.	n.a.	n.a.	n.a.	0.32	n.a.	n.a.	0
As	47.14	46.77	48.56	46.62	n.a.	n.a.	0	0	n.a.	n.a.	0
Sb	0.06	0	0.27	0	n.a.	n.a.	0	0	n.a.	n.a.	0
S	18.36	18.13	16.14	19.2	n.a.	n.a.	0	0	n.a.	n.a.	0.17
Total	100.58	99.63	99.00	100.66	100	100	98.49	99.89	100	100	96.42
	Coefficients of crystal chemical formula										
Fe	0.331	0.303	0.222	0.166	0.022		0.005	0.005	0.018	0.024	0.005
Co	0.088	0.249	0.171	0.561	0.000		0.000	0.001			0.000
Ni	0.590	0.457	0.618	0.251	0.000		0.002	0.000	0.006		0.000
Cu	0.000	0.000	0.004	0.000	0.020		0.000	0.000			0.000
Ag	0.000	0.000	0.000	0.000	0.440	0.233	0.245	0.063	0.092	0.104	0.455
Au	0.000	0.000	0.000	0.000	0.519	0.767	0.748	0.925	0.884	0.872	0.532
Hg					0.000			0.003			0.000
As	1.047	1.049	1.124	1.019			0.000	0.000			0.000
Sb	0.001	0.000	0.004	0.000			0.000	0.000			0.000
S	0.952	0.951	0.873	0.981			0.000	0.000			0.008

n.a., not analyzed.

sporadically increases up to 0.5–2.0 ppm (Figs. 8, 10); however, we most likely are dealing here with a series of small lenses related to zones of carbonation, silicification, and recrystallized arsenopyrite.

In the central block of studied area (sections 3–3, 4–4), where biotite–calcite and chlorite–calcite metasomatic rocks are not recorded, although tectonization (minor folding, brecciation) and metasomatic alteration of rocks (primarily, silicification, as well as carbonation) are expressed intensely, the gold mineralization at the boundary between chlorite–actinolite and hornblende is not recorded. Above the indicated boundary, in the altered hornblende amphibolite similar to that in the western block, separate intervals with Au grade of >1 gpt have been revealed.

Although a link between sulfoarsenides and gold is undoubted, a direct relationship between As and Au contents is not established. Thus, for the selection of Au-bearing samples (>0.25 ppm Au, 99 samples), the arithmetical mean gold contents for a series of As contents: <0.1, 0.1–0.25, and >0.25% turned out to be practically equal: 1.11, 1.15, and 1.11 ppm, respectively.

Native gold in polished sections is identified relatively frequently, being recorded at ≥0.1 gpt Au in rock. Thus, it may be supposed that the share of finely dispersed gold in sulfides and sulfoarsenides is not high, and this has been confirmed by laboratory study of ore for its dressability. A gold microinclusion (judging by straw-colored, this is electrum) has been detected in pyrrhotite near its contact with chalcopyrite only in one case. In all other cases, gold segregations are related to sulfoarsenides. The most common are gold grains at the boundary between arsenopyrite and gersdorffite with gange minerals (chlorite, actinolite, biotite, quartz) (Fig. 12) as well as in gangue minerals close to sulfoarsenide grains. The predominant gold grains are 10–40 μm in size; the maximum size of gold particles is 0.1 mm. The shape of particles is isometric and clotted.

In addition, gold microinclusions in arsenopyrite are recorded as disseminated grains and recrystallized metacrystals in contact zones of quartz and quartz–carbonate veinlets (Fig. 12). Microinclusions of gold up to a few μm are recorded in gersdorffite.

In Au-bearing samples, the accessory scheelite has been identified along with galena, which, like gold, is formed at contacts of arsenopyrite and gersdorffite with gangue minerals or along fractures in sulfoarsenides. Micrograins of ullmannite and hessite are detected together with gold.

Gold from lenses of arsenopyrite mineralization in the sequence of hornblende amphibolites (microinclusions in arsenopyrite and segregations at the boundary of arsenopyrite grains with gangue minerals) are of low fineness (~655‰), see Table 3. Gold from the main ore zone in hornblende amphibolite is predominantly characterized by high fineness (957‰, average of 16 analyses) and partly by medium fineness (average 792‰, five analyses). In chlorite–actinolite rocks, gold is characterized by medium fineness (average 814‰, 20 analyses) and less frequently by low fineness (672‰). In addition to silver, the microadmixtures of Fe (up to 0.17%), Ni (up to 0.05%), and, in one case, Hg (0.32%) have been recorded (Table 3).

Thus, gold mineralization is superimposed and its distribution comprises interrelated elements of stratigraphic, metasomatic, and geochemical controls. The stratigraphic control is expressed in the relation of gold to the lower part of hornblende and to the upper part of chlorite–actinolite amphibolites; the main mineralized zone is localized immediately at the boundary between these sequences. Metasomatic control implies the connection of gold mineralization to the areas of intense metasomatic alteration of rocks. The main mineralized zone is controlled by biotite–calcite metasomatic rocks. At the same time, the gold content does not depend on the protoliths, after which the metasomatic rocks are developed, i.e., petrographic control does not work. The geochemical control is expressed in the confinement of gold to zones of sulfoarsenides—arsenopyrite in the sequence of altered hornblende amphibolite and porphyritic diorite as well as gersdorffite and arsenopyrite in chlorite–actinolite amphibolite. Geochemical association of gold mineralization is Au–As–(Ni).

To estimate the age of gold mineralization in Sergozero ore occurrence, a sample of slightly altered porphyritic diorite dike has been taken from borehole SRG-9 at the spot elevation of 65 m (Fig. 8a). This dike crosscuts metavolcanic rocks of the Sergozero Sequence. Porphyritic diorite is the youngest rock of the Sergozero ore occurrence containing gold mineralization. Therefore, using this rock, we can determine its lower age boundary. Zircons in porphyritic diorite are represented by dipyramidal–prismatic transparent crystals (elongation coefficient is 3.0–4.5); facets {100}, {110}, and {111} are predominant; facet {311} is also observed on certain crystals (Fig. 13). The color of crystals is brown; the luster is vitreous. Zircon grains are fractured and frequently contain inclusions of other minerals. The internal structure of crystals is characterized by fine zoning of growth (Fig. 13). Gray color in the image in the regime of back-scattered electrons (BSE) denotes insignificant zones of zircon alteration. They emphasize growth zoning and are localized at outer boundaries of grains (Figs. 13c, 13d). The age was measured using the U–Pb method (TIMS) applied to the least altered zircon grains various in size and without visible inclusions (Table 4). Analytical points of isotopic composition of five zircon fractions lie in discordia with the age 1874 ± 3 Ma at the upper intersection with concordia; MSWD = 0.74; the lower intersection with age of 7 ± 110 Ma reflects contemporary losses of lead (Fig. 14). The obtained value of 1874 ± 3 Ma corresponds to the time of zircon crystallization from melt during the emplacement of dikes. Taking into consideration the

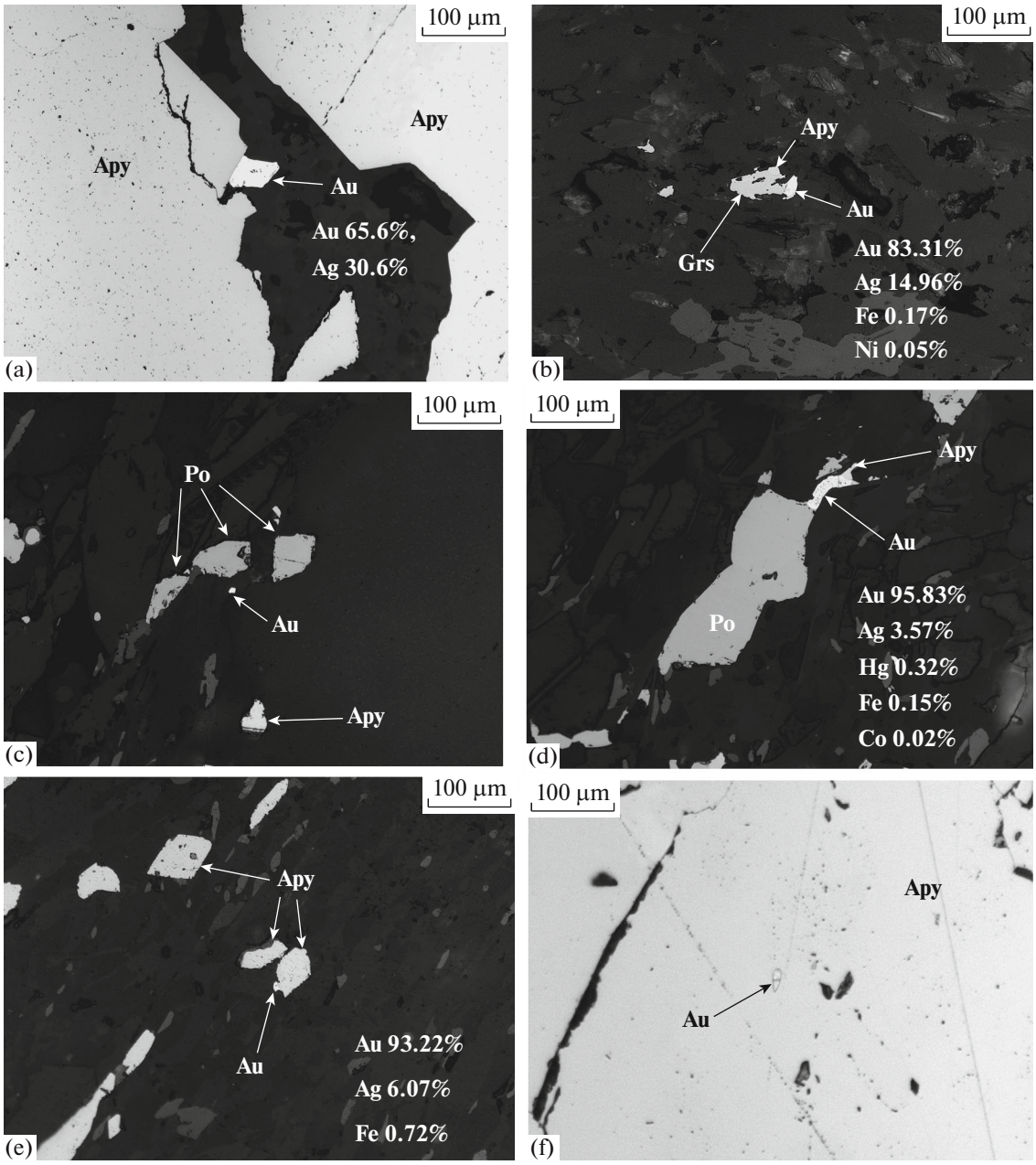

Fig. 12. Gold in intergrowths with arsenopyrite and gersdorffite. Reflected light, parallel polars: (a) electrum in quartz along fracture in arsenopyrite, (b) gold at the boundary of gersdorffite and silicate minerals; (c) gold in quartz near pyrrhotite and arsenopyrite; (d) gold in the intergrowth with pyrrhotite and arsenopyrite; (e) gold at the boundary of arsenopyrite and gangue minerals; (f) gold microinclusion in arsenopyrite. Composition of gold grains was determined with an MS-46 CAMECA, see Table 3. Apy—arsenopyrite, Au—native gold, Grs—gersdorffite, Po—pyrrhotite.

liaison of gold with biotite–calcite metasomatic alteration superimposed on all rocks of Sergozero ore occurrence, including porphyritic diorite, we can concluded that gold mineralization was formed after the intrusion of the dike dated at 1874 ± 3 Ma.

To estimate the age of wall-rock alteration with which gold ore formation is related, the isotopic composition of superimposed minerals and whole-rock sample were studied using the Rb–Sr method. The isochron age of muscovite, calcite, apatite, plagioclase, clinozoisite, and whole rock sample (WR) of the porphyritic diorite is 1739 ± 89 Ma; MSWD = 1.4 (Table 5; Fig. 15). This estimate allows us to bring metasomatic transformation of rock and ore formation into correlation with the retrograde stage of Svecofennian metamorphism. The obtained age is consistent with the suggested time of intracontinental collision during formation of the Lapland–Kola–Belomorian

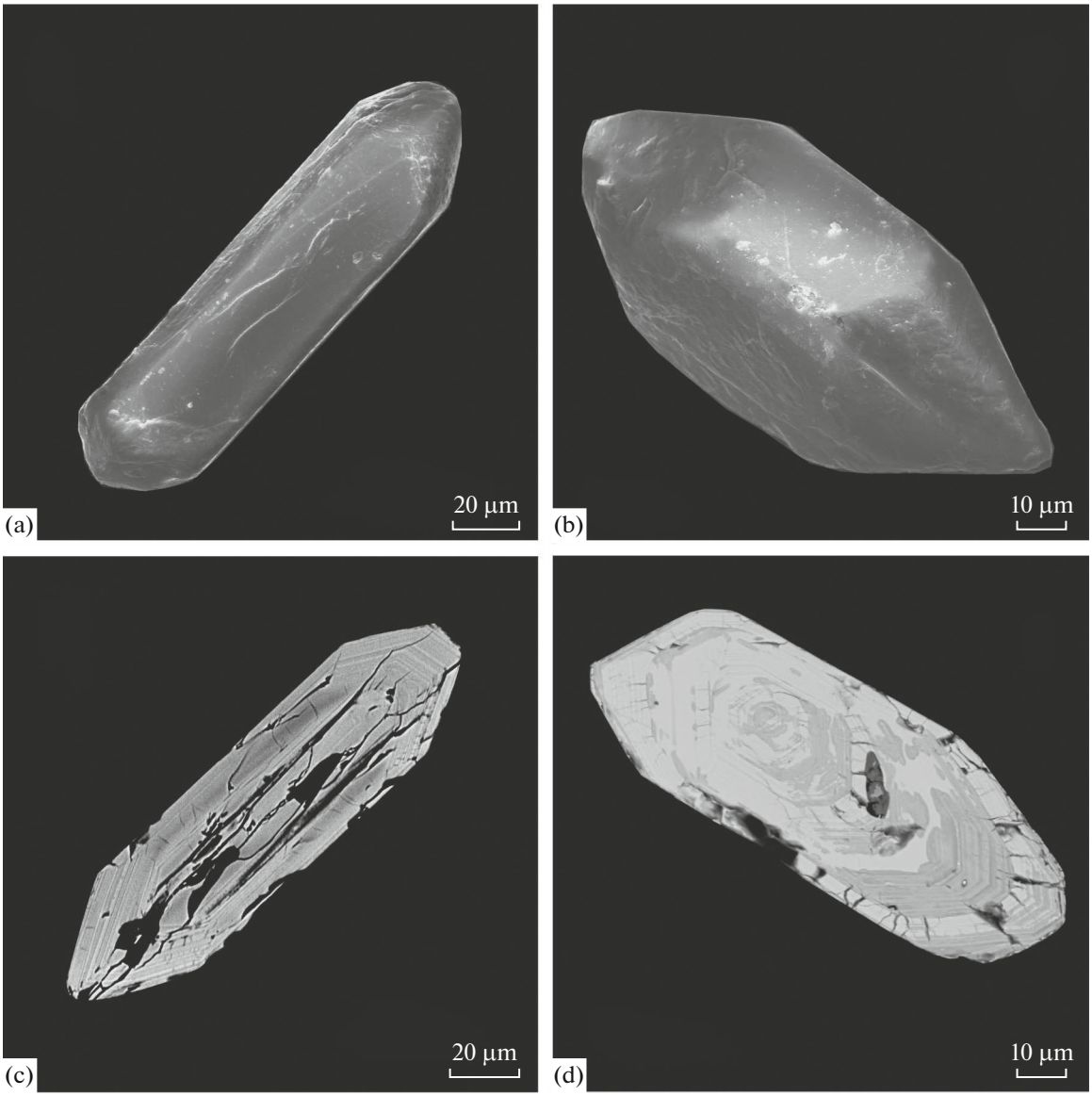

Fig. 13. Photomicrographs of zircon crystals from porphyritic diorite of Sergozero ore occurrence: (a, b) REM images; (c, d) images in reflected electrons

Orogen (1.87–1.70 Ga), as is shown by *Glubinnoe Stroenie* ... (2010), and with age of metasomatic alteration of biotite gneiss of the Pyalochny Sequence, which has been estimated with the U–Pb method, as related to time interval 1830–1750 Ma (Astaf'ev et al., 2010).

DISCUSSION

The main features of geological structure of the Vorgovy and Sergozro ore occurrences—in particular, localization of mineralization in the zone of viscous deformations and metasomatic reworking of host metamorphic rocks; connection of mineralization with zones of quartz, carbonate–quartz, and carbonate veinlets; sulfide impregnations in metasomatically altered rocks; relatively low content of sulfides; lack of obvious link with intrusive bodies—all this allows us to refer occurrences to the class of "orogenic" gold ore objects (Groves et al., 2003; Goldfarb et al., 2001).

The studied ore occurrences are situated in the zone of tectonic contact of two large greenstone structural units in the Kola region: the Neoarchean SBG and the Paleoproterozoic IVZ. The control of arrangement of gold ore fields by large trans-crustal faults of the first order, which serve as transport ways during the migration of ore-bearing fluids, is typical of "orogenic" gold deposits and widely covered in the literature (Eisenlohr et al., 1989; Witt and Vanderhor, 1998). With all this going on, it is indicated that ore

Table 4. Results of U–Pb isotopic study of zircon from porphyritic diorite of the Sergozero ore occurrence

Sample, fraction number	Size of fraction, μm charge, mg	Content, μg/g		Isotope ratios					Rho	Age, Ma		
		Pb	U	$^{206}Pb/^{204}Pb^*$	$^{207}Pb/^{206}Pb^*$	$^{208}Pb/^{206}Pb^*$	$^{206}Pb/^{238}U$	$^{207}Pb/^{235}U$		$^{206}Pb/^{238}U$	$^{207}Pb/^{235}U$	$^{207}Pb/^{206}Pb$
SRG-9/1	+100, 0.6	230	663	1856	0.1219 ± 1	0.07191 ± 3	0.3361 ± 5	5.231 ± 10	0.78	1868 ± 3	1872 ± 4	1877 ± 3
SRG-9/2	−100 + 75, 0.8	214	620	1908	0.1216 ± 1	0.07210 ± 5	0.3344 ± 8	5.285 ± 15	0.91	1859 ± 5	1866 ± 6	1874 ± 3
SRG-9/3	−75 + 50, 0.5	336	947	987	0.1280 ± 1	0.09597 ± 2	0.3317 ± 5	5.238 ± 13	0.71	1847 ± 3	1859 ± 5	1872 ± 3
SRG-9/4	+75, 0.3	248	793	1575	0.1231 ± 1	0.07842 ± 7	0.3008 ± 6	4.759 ± 12	0.75	1695 ± 3	1778 ± 4	1876 ± 3
SRG-9/5	−50, 0.4	245	755	1687	0.1223 ± 1	0.07559 ± 7	0.3133 ± 6	4.945 ± 12	0.76	1757 ± 4	1810 ± 5	1872 ± 3

* Values are corrected for mass-fractionation, blank contamination and common lead, according to the model by Stacey and Kramers (1975). All uncertainties are given at level 2σ and correspond to the last significant figures after the comma.

objects are related, as a rule, to the fault zones of second–third orders, which are characterized by favorable conditions for ore deposition rather than to the main fault (McCuaig and Kerrich, 1998; Neumayr et al., 2000; Neumayr and Hagemann, 2002). Gold deposits are also known immediately in mentioned main faults of the first order, but they are sporadic and with few exceptions are not large. For example, these are Lapa, Orenda, and Malartic deposits in the Cadillac Fault Zone, which separates the Abitibi Belt from the Pontiac Subprovince in the Superior Province, Canada (Neumayr and Hagemann, 2002; Simard et al., 2013). It should also be noted that particularly the age of tectonic movements, which gives rise to mass migration of ore-bearing fluids through fault zones, rather than age of host rocks defines the time of ore formation, which commonly corresponds to peak of regional metamorphism or its regressive stage.

The Sergozero occurrence is located 1.5–2.0 km from the reverse fault zone, which upthrows Archean complexes of SGB over Paleoproterozoic sequences of IVZ and is controlled by local faults, which are nearly parallel to the main tectonic zone. In other words, its geological position is typical of orogenic deposits. The Vorgovy occurrence is situated immediately within the reverse fault zone at the contact between SGB and IVZ.

The role of crosscutting Kolmozero–Strelna Fault in formation of mineralization in the studied occurrences remains ambiguous. However, as was said above, blocks to the west and to the east of this fault were apparently taken out at different levels of erosion truncation. If we judge by an abrupt disappearance of geochemical gold anomalies in the Sosnovka–Strelna domal fold zone (Fig. 4), the tectonic movements along the fault took place later than ore formation.

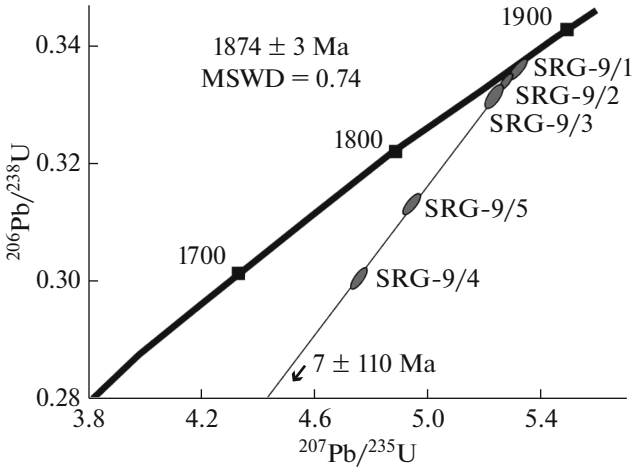

Fig. 14. Diagram with concordia for porphyritic diorite from the Sergozero ore occurrence.

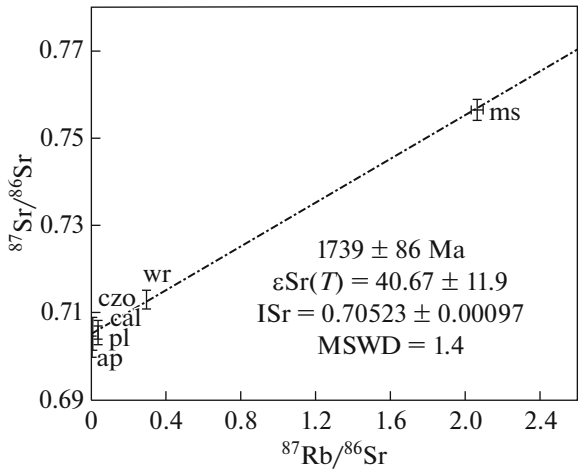

Fig. 15. Rb–Sr isochron for porphyritic diorite from the Sergozero ore occurrence. ap, apatite; cal, calcite; czo, clinozoisite; pl, plagioclase; ms, muscovite; wr, whole-rock sample.

Table 5. Rb–Sr isotopic data of minerals superimposed on porphyritic diorite dike at the Sergozero ore occurrence

Mineral	Content, mg/g		Isotope ratio			$I_{Sr}(1739)$	$\varepsilon_{Sr}(1739)$
	Rb	Sr	$^{87}Rb/^{86}Sr$	$^{87}Sr/^{86}Sr$	±Δ		
Apatite	0.61	482.0	0.003571	0.70386	14	0.70377	19.8
Plagioclase	13.11	1169.2	0.031636	0.70508	18	0.70429	27.2
Calcite	9.21	798.8	0.032530	0.70621	16	0.7054	43.0
Clinozoisite	2.14	1804.3	0.003346	0.70707	12	0.70699	65.6
Whole rock sample (WR)	73.27	702.7	0.294185	0.71318	19	0.70583	49.1
Muscovite	149.34	204.2	2.063408	0.75672	21	0.70513	39.2

The basic elements of geological–genetic model of the Sergozero occurrence are listed below:

(1) Confining of mineralization to volcanic rocks corresponding to komatiite, komatiitic and tholeiitic basalts in composition.

(2) Stratigraphic control of mineralization: localization of the main mineralized zone in contact zone between komatiitic and tholeiitic basalts.

(3) The host rocks are metamorphosed under conditions from higher greenschist to epidote-amphibolite facies. Ultramafic rocks are transformed into chlorite–actinolite (±talc) aggregate and mafic rocks are transformed into hornblende amphibolite.

(4) Tectonization of rocks in contact zone is expressed mainly in viscous deformations: plication and local brecciation.

(5) Intense hydrothermal metasomatic alteration of amphibolites and gneisses (silicification; formation of chlorite–calcite, biotite–calcite, and other metasomatic rocks; graphitization of rocks).

(6) Superimposed character of mineralization: Au-bearing biotite–calcite metasomatic rocks develop after protoliths various in composition and age (Neoarchean mafic–ultramafic metavolcanic rocks and Paleoproterozoic porphyritic diorite). Potassic metasomatism (biotitization) along with the appearance of arsenopyrite disseminations serves as an important attribute of gold mineralization at ore occurrence.

(7) Ore lenses and complex ore zones are 1–12 m in thickness and a few hundred meters in extent.

(8) Predominant free native gold is in association with sulfoarsenides: arsenopyrite and gersdorffite.

In the Russian part of the Fennoscandian Shield, the Rybozero ore occurrence in southeastern Karelia is the closest to Sergozero in typification (Kuleshevich, 2013; *Mineral'no* ..., 2005), whereas the ore objects of this type were not recorded earlier in the Kola region.

The characteristics of Sergozero ore occurrence listed above have been taken into consideration for the choice of similar objects among well-studied deposits. The operating "orogenic" gold deposits, where gold is related to altered mafic and ultramafic metavolcanic rocks, are localized in the Fennoscandian Shield and in Archean greenstone belts of Canada, Australia, Indian, and South Africa. The host rocks at a majority of these deposits have been metamorphosed under conditions of greenschist facies. The following deposits are listed below as examples. These are deposits from the Superior Province in Canada: Campbell Red Lake and Madsen in the Uchee Belt; Timins, Larder Lake, and Cadillac deposits in the Abitibi Belt (Dube et al., 2004; Dube and Gosselin, 2007); Mount Sharlotte and Golden Mile in the Norseman-Wiluna Belt, Yilgarn Craton in Australia (Witt and Vanderhor, 1998), and many others. Gold is hosted therein in carbonate (ankerite, dolomite, and less abundant calcite), carbonate–quartz, and quartz veins and veinlets. If metamorphism of host rocks at "orogenic" deposits rises to the level of high greenschist or amphibolite facies, then they are characterized by impregnated gold mineralization in metasomatically altered rocks rather than gold-bearing veins or veinlets. For example, such are the Norseman and Coolgardie groups of deposits, Yilgarn Craton (Witt and Vanderhor, 1998), or Lapa in the Abitibi Belt in Canada (Simard et al., 2013).

The Archean and Proterozoic economic gold deposits and tens of perspective occurrences are clustered in the Finnish part of the Fennoscandian Shield. Here one may mention the Neoarchean Ilomantsi Greenstone Belt, the southern framework of Paleoproterozoic Central Lapland Greenstone Belt (CLGB), and Kittilä Shear Zone in its central part. The latter zone is marked by localization of the Suurikuusikko large gold deposit, a single in the Fennoscandian Shield.

The Ilomantsi Greenstone Belt, which is located in eastern Finland, is represented by an Archean meridional structural unit passing to the adjacent territory of Russia, where it is called Kostomuksha Greenstone Belt. In the 35-km segment of the Ilomantsi Belt adjoining the Finland–Russia border, 23 gold ore objects have been revealed; one of them (Pampalo deposit) is in operation currently; six other objects are objects of geological exploration, including pilot mining. This area is known as the Karelian Gold Line (Eilu, 2009). The host rocks, among which are the rel-

atively abundant intermediate and felsic volcanic and volcano-clastic rocks, were metamorphosed 2750–2700 Ma ago under conditions of the lower amphibolite facies (T = 550 ± 50°C). The leading factors, which control localization of ore objects within the greenstone belt, are narrow (a few hundred meters in width) shear zones oriented in the direction of the structure long axis and related to the stage of maximum metamorphic events (Eilu, 2009). In particular, the Ward area of the largest Pampalo gold deposit is confined to the core of the fold extending along the shear zone of the same name. This structural unit is an area of local extension against the background of compression and shear that focuses the flow of medium-temperature ore-bearing solutions. The deposits and ore occurrences are not governed by lithologic control: the orebodies proper may accommodate in both metamorphic rocks and minor intrusions variable in composition. A certain statistic trend is recorded for the ore objects that are clustered in fields of metapelitic muscovite–quartz schists and, to a lesser degree, in tonalitic intrusions. Mineralization cross-cuts boundaries of lithologic and petrographic subdivisons, mainly concentrating at boundaries of rock complexes. In various cases, one can observe orebodies conformable to the attitude of metamorphic rocks and distinctly cross-cutting them. Infiltration of fluids is controlled by sufficiently wide zones of rock deformation, and this is reflected in impregnated rather than vein mineralization. At all ore objects of the belt, chloritization, tourmalinization, and muscovitization are predominant metasomatic alterations; albitization and carbonation are supplemented at the Pampalo deposit. Geochemical association of gold mineralization is Au–As–Bi–Te–B–Cu–Ag–Mo–W.

The age of mineralization (2708–2693 Ma) corresponds to the peak of metamorphism, but the role of Paleoproterozoic events (1.9–1.8 Ga) is not ruled out (Poutiainen and Partamies, 2003). Gold is largely fine (<15 μm), free, and occurs among silicates, either as intergrown with pyrite and pyrrhotite and less frequently with arsenopyrite or rutile; intergrowths of gold with Bi, Ag, Fe tellurides, native bismuth, and Au tellurides occur as well.

The group of gold deposits and occurrences developed along the southern boundary of the Proterozoic rift structure of the Central Lapland Greenschist Belt (CLGB) related to the Sirkka Shear Zone comprises the operating Saattopora deposit, 11 not operating small deposits and ore occurrences, and 13 objects that do not possess estimates of resources. The well known Suurikusikko and Pahtavaara deposits are not included in this group. They are located in the central part of the belt beyond the considered shear zone (*Gold* ..., 2007). The Sirkka Shear Zone is a series of thrust faults that bound the area of Proterozoic greenstone rocks in the south. The shear zone is traced across the western part of Finnish Lapland from Muonio to Sodankyla. The ore objects are localized either immediately within the Sirkka Shear Zone or nearby it at a distance of 3 km and are related to the fault zones of a lower order. As a rule, the gold mineralization forms series of ore lenses parallel to stratification near boundaries of metakomatiites and metatholeiitic basalts with metasedimentary rocks mainly represented by phyllites. The host supracrustal rock complexes are metamorphosed predominantly under conditions of greenschist facies and less frequently of lower amphibolite facies. The hydrothermal metasomatic transformation includes (i) albitization or scapolitization at the pre-ore stage, (ii) sericitization and carbonation at ore formation under conditions of lower–middle greenschist facies, and (iii) biotitization and carbonation under conditions of upper greenschist—lower amphibolite facies. The deposits from belt are grouped into two categories: (1) gold ore objects proper and (2) deposits and occurrences of copper–gold mineralization; the latter are characterized by a higher grade of metamorphism. The ore mineralization is related to carbonate–quartz and quartz–carbonate veins; ankerite and dolomite are predominant carbonates. Geochemical specialization of mineralization: Au–Cu–As–(Ag–Pb–Zn–Ni). The age of mineralization is estimated at 1900–1811 Ma ago (*Gold* ..., 2007).

The main sulfide minerals accompanying native gold are pyrite, pyrrhotite, and, in some cases, arsenopyrite and gersdorffite. Native gold is contained in the gold deposits proper; both free gold (no less than 32%) and that fixed in sulfides (in pyrite and less in chalcopyrite) are contained in Au–Cu deposits.

The Suurikuusikko deposit is situated in the central part of CLGB in the Kiistala Shear Zone, which is a lateral near-meridional branch of the regional Sirkka Shear Zone (*Gold* ..., 2007). The deposit is hosted in rocks of the Kittilä Series with an age of 2.02 Ga ago. Tholeiitic basalts dominate in this series. The major ore zone is oriented in a near-meridional direction. To the west of main ore zone, the sequence of massive and pillow-lavas occur. In the ore zone proper, they give way to andesitic lavas and intermediate pyroclastic rocks. Mineralization is commonly related to pyroclasts or volcanics with attributes of extrusions. On the eastern side of the main ore zone, the sequence of predominant metasedimentary rocks occurs, including jaspilite or banded iron formation (BIF) and black shale, which are changed with mafic and ultramafic lavas. The mafic metavolcanic rocks are chloritized in the outer part of the metasomatic aureole. In the ore zone, the rocks underwent intense pre-ore albitization and carbonation (calcite, dolomite) at the productive stage.

The geochemical specialization of mineralization: Ag, As, Au, Bi, Co, Sb, W. Four stages are recognized in the development of mineralization at the Suurikuusikko deposit. Gold is related to the second stage characterized by arsenopyrite and pyrite crystalliza-

tion. The greater part of gold (73.2%) falls on arsenopyrite and the least part on arsenic pyrite (22.7%), and only a small share is represented by free gold. Gold is submicroscopic; its inclusions are recorded in pyrite and are rare in arsenopyrite. The Re–Os age of mineralization is 1916 ± 19 Ma (Au-bearing arsenopyrite) and corresponds to the period of thrusting in the Central Lapland Belt (*Gold* ..., 2007). Thus, a gap in time between deposition of volcanic and sedimentary rocks and formation of mineralization amounts to 60–100 Ma.

In comparison of Sergozero occurrence with the described objects in greenstone belts of Finland, one may state that the former is related to another type of ore objects than counterparts from the Ilomantsi Belt. The distinctions are as follows:

(1) in composition of host rocks;

(2) in character of metasomatic alterations;

(3) in association of chemical elements at productive stage;

(4) in ore mineralogy; and

(5) in age of mineralization.

The Sergozero occurrence also substantially differs from the Suurikuusikko deposit in the above attributes except for age of mineralization. At the same time, the Sergozero occurrence possesses a number of common features with ore occurrences and deposits localized in the Sirkka Shear Zone of CLGB:

(1) Tectonic position in the regional shear zone (in the case of Sergozero occurrence, this is the South Varzuga Fold Zone, which accompanies the upthrow zone of rocks belonging to the Sergozero Sequence of the Lopian Complex (2766 ± 15 Ma) over Paleoproterozoic (Sumian) sequences of the Strelna Series in IVZ (2424 ± 5 Ma); in CLGB, this is the Sirkka Shear Zone, i.e., a series of thrust faults of Paleoproterozoic Sodankyla and Savukoski complexes (2.05 Ga) over rocks of the Kittilä Complex (2.00 Ga).

(2) Stratigraphic and lithologic factors of control: The main mineralized zone of the Sergozero ore occurrence is related to the contact zone of the komatiitic member with overlying tholeiitic basalts, whereas mineralization is localized at the contact of komatiitic member with tholeiitic basalts or initially sedimentary rocks (phyllites) in occurrences of the Sirkka Shear Zone.

(3) Metamorphism of host complexes of the Sergozero occurrence corresponds to conditions of the higher greenschist–epidote-amphibolite facies. The grade of regional metamorphism of host rocks in the majority of ore objects of CLGB is related to the lower and middle levels of greenschist facies but reaches the high level greenschist to the lower level of amphibolite facies at certain objects.

(4) The superimposed character and age of mineralization: the gold mineralization was formed at the regressive stage of the Svecofennian regional metamorphism. For the Sergozero ore occurrence, we suppose an age of 1.7–1.8 Ga, whereas the ages are 1.79–1.85 Ga for ore occurrences from CLGB.

(5) Gold is associated with arsenopyrite in ore, while with gersdorffite and cobaltite in rocks enriched in Ni and Co, respectively. Gold is commonly free and of high fineness.

Differences of the Sergozero occurrence from deposits and occurrences of CLGB consist in the following features:

(1) In character of metasomatic alteration of ore-bearing rocks. At most ore occurrences of CLGB, the rocks underwent intense preore albitization, and the crucial wall-rock alterations are sericitization, carbonation, and silicification. At the Sergozero ore occurrence, albitization is not recorded at all, while predominant alterations are biotitization and silicification. Nevertheless, the objects with biotitization and carbonation are also known; these are the Kaaresselkä and Pahtavaara occurrences (Eilu, 2009; *Gold* ..., 2007), i.e., those where grade of metamorphism is higher than elsewhere and corresponds to the higher level of greenschist facies.

(2) In texture of mineralization. In CLGB, gold is largely related to the echeloned carbonate-quartz and quartz–carbonate veins, in contrast to impregnated mineralization in metasomatically altered rocks at the Sergozero occurrence.

(3) In mineralogy of ore. At the occurrences of CLGB, pyrite is the major ore mineral. At the Sergozero occurrence, the leading role belongs to pyrrhotite and arsenopyrite; pyrite is sporadic and commonly is a late superimposed mineral.

All differences listed above may be explained by the higher grade of host rock metamorphism and higher temperature of ore formation at the Sergozero ore occurrence. Various ages of host rocks are not principal, because compositions of rock complexes are close and gold mineralization in both cases is superimposed and was formed at the regressive stage of the Svecofennian metamorphism.

The deposits similar in their characteristics with Sergozero occurrence are also known in the Archean greenstone belts of Canada, Australia, and South Africa. The Lapa, one of these deposits, is localized within the Cadillac–Larder Lake Fault Zone, which divides Abitibi (2685–2710 Ma) and the Pontiac subprovinces (≤2685 Ma, Davis et al., 2002) of the Superior Province, Canada (Simard et al., 2013). Along this fault zone, the member of metavolcanic rocks consisting of tholeiitic basalt, porphyritic andesite, calc–alkaline tuff, and komatiite is traced as a tract less than 2 km in width among metasedimentray rocks. The metavolcanic rocks are cross-cut by felsic and basic dikes. This member controls localization of gold deposits belonging to the Cadillac Group, including the Lapa deposit. The gold deposits are hosted in metavolcanic rocks from ultramafic to felsic in composition, as well as metasedimentary biotite schists.

Ultramafic rocks play the leading role. Metamorphism at the Lapa deposit is zonal. At the upper level of the deposit, the rocks are metamorphosed under conditions of greenschist facies and of lower amphibolite facies at a depth below 1000 m (Simard et al., 2013). According to classification of metamorphic facies accepted in Russia, they correspond to epidote-amphibolite facies. The age of metamorphism is estimated at 2677–2643 Ma (Ayer et al., 2002). During retrograde metamorphism (2645–2415 Ma), the ore-bearing rocks underwent intense deformations, largely viscous, and metasomatic alteration (Simard et al., 2013). The newly formed biotite, quartz, dolomite, calcite, tourmaline, and chlorite develop in the upper part of deposit, and chloritization is predominant in the outer zones of aureoles. At a depth of more than 1 km, the main superimposed mineral is actinolite, which develops together with biotite, chlorite, albite, and tourmaline. The early generation of finely impregnated Au-bearing arsenopyrite is formed synchronously with biotitization. Recrystallization of this arsenopyrite at later stages leads to the release of gold and the formation of gold inclusions in the newly formed porphyroblastic arsenopyrite and to the separation of native gold at boundaries of arsenopyrite and pyrrhotite, in quartz veinlets, and in porphyroblastic grains of newly formed hornblende, biotite, and actinolite. Assemblage of ore minerals and geochemical specialization of mineralization also vary with depth depending on metamorphic grade of rocks. For example, antimony minerals (aurostibite, antimonite, gudmundite) are recorded in rocks of greenschist facies together with gold and arsenopyrite. In rocks that underwent metamorphism of amphibolite facies, these minerals disappear.

Thus, the complex of host rocks; the level of regional metamorphism of host rocks, texture and structure, mineralogy; and association of chemical elements of mineralization of the Sergozero occurrence and the Lapa deposit are comparable in many features, although certain distinctions are also recorded. In particular, albitization and tourmalinization are not typical of the Sergozero occurrence and antimony mineralization is practically not identified.

Classification of the Sergozero occurrence as a gold ore object of the "orogenic" type and comparison with well-studied objects-analogs allow us to expect that gold mineralization is not limited by a small studied area but spreads along the entire tectonic contact between SGB and IVZ to a great depth, e.g., at the Lapa deposit mineralization has been traced down to 1500 m (Simard et al., 2013) and down to 1600 m without indications of wedging out at the New Consort deposit in the Barberton Belt, South Africa (Otto et al., 2007). The areas of economic mineralization may alternate with mineralized intervals of subeconomic significance. The complex geometry of mineralized space, when individual orebodies a few meters in thickness and a few hundred meters in extent make up complexly built ore zones traced for several kilometers is one of characteristic features of "orogenic" deposits. The perspective of tectonic contact between SGB and IVZ for a significant extent is confirmed by geochemical mapping of the territory (Fig. 4). The connection of mineralization to komatiite, as a component of metamorphic complex, allows us to use mapping of ultramafic volcanic rocks, including their geochemical characteristics (Cr, Ni), as an efficient prospecting tool.

CONCLUSIONS

(1) Gold ore occurrences have been revealed in Sergozero Block of the Strelna Greenstone Belt. Accommodation of occurrences is controlled by tectonic contact between Neoarchean sequences of the greenstone belt and Paleoproterozoic volcanic and sedimentary rocks of the Imandra–Varzuga Zone.

(2) The Sergozero gold ore occurrence is related to the member of mafic–ultramafic metavolcanic rocks among biotite and muscovite–biotite gneisses (metapelites). The mineralized zone up to 80 m in thickness encompasses the upper part of the chlorite–actinolite amphibolite sequence (former komatiite and komatiitic basalt) and the lower part of the overlying hornblende amphibolite (former tholeiitic basalt).

(3) Mineralization is related to the conformable shear zone of intense metasomatic transformation of rocks. The crucial mineralized zone is confined to the strip of biotite–calcite metasomatic rocks after various protoliths: chlorite–actinolite, hornblende amphibolites, and cross-cutting porphyritic diorite dikes. Upsection, separate thin lenses with gold–arsenopyrite mineralization have been revealed in silicified and carbonated hornblende amphibolite.

(4) Gold is related to disseminated sulfoarsenide mineralization represented by arsenopyrite and gersdorffite. Gold most frequently crystallizes along boundaries of arsenopyrite and gersdorffite grains with silicates, including quartz, while less frequently along fractures and boundaries of silicate grains and inclusions in arsenopyrite. Gold is fine, and size of isometric and lumpy grains is predominantly 25–40 μm, 0.1 mm as a maximum. Gold varies from low (655–670) to high (930–960) fineness; Fe and Ni admixtures are identified, and Hg in one case.

(5) Formation of gold mineralization is related to regressive stage of the Svecofennian metamorphism. The lower age limit of gold mineralization is determined by the age of porphyritic diorite dike, which is the youngest known ore-bearing rock: the age of magmatic zircon from this rock is 1874 ± 3 Ma (U–Pb method). The Rb–Sr age of metasomatic alteration of porphyritic diorite has been estimated at 1739 ± 86 Ma.

(6) The main characteristics of the studied occurrences: relation of mineralization to the zone of viscous deformations and alteration of host metamorphic

rocks; links of mineralization to zones of quartz, carbonate–quartz, and carbonate veinlets and sulfide disseminations; relatively low contents of sulfides in ore-bearing rocks; lack of an obvious link with intrusive bodies—all these features allow us to put the studied ore occurrences to the class of "orogenic" gold ore objects.

(7) Comparison of ore occurrences in the Strelna Greenstone Belt with operating gold deposits in the Fennoscandian Shield (Finland) and the Superior Province in Canada similar in characteristics provides evidence for the perspective of the Strelna Belt for gold deposits.

ACKNOWLEDGMENTS

We thank O.V. Menchinskaya (Institute of Mineralogy, Geochemistry, and Crystal Chemistry of Rare Elements, Moscow), G.V. Ruchkin and V.B. Chekvaidze (Central Institute of Geological Exploration for Base and Precious Metals, Moscow) for their consultations, and L.I. Koval and the staff of Laboratory for Matter Separation for preparation of mineral monofractions (Geological Institute, Kola Science Center, Apatity). We are grateful to Yu.G. Safonov for fruitful discussion and thank reviewers for their comments. This work was carried out under project 0231-2015-0001 and PRAN 1.4 Program; isotopic geochemical study was supported by the Russian Foundation for Basic Research, project nos. 14-05-00443 and 16-05-00367.

REFERENCES

Astaf'ev, B.Yu. and Voinova O.A., Composition, age, and genesis of rocks of the Tersky greenstone belt (Kola Peninsula), in *Magmatizm i metamorfizm v istorii Zemli: Tezisy XI Vseross. petrograficheskogo soveshchaniya* (Magmatism and Metamorphism in the Earth's Evolution. Proceedings of 11th Petrographic Conference), Ekaterinburg, 2010, pp. 61–62.

Astaf'ev, B.Yu., Voinova, O.A., Levskii, L.K., and Voinov, A.S., New data on dating of metamorphic and metasomatic rocks of the Tersky greenstone belt (Kola Peninsula), in *Sovremennye problemy magmatizma i metamorfizma: Mater. Vseross. konf., posv. 150-letiyu akademika F.Yu. Levinsona-Lessinga i 100-letiyu professora G.M. Saranchinoi* (Modern Problems of Magmatism and Metamorphism. Proceedings of All-Russia's Conference dedicated to the 150th Anniversary of F.Yu. Levinson-Lessing and 100th Anniversary of Professor G.M. Saranchin), St.-Petersburg: SPbGU, 2012, vol. 1, pp. 51–53.

Astaf'ev, B.Yu., Levchenkov, O.A., Rizvanova, N.G., Voinova, O.A., Voinov, A.S., Levskii, L.K., Makeev, A.F., and Lokhov, K.I. Geological Structure and Isotopic–Geochronologic Study of Rocks from the Strel'na Segment of the Terskii Greenstone Belt, Kola Peninsula, *Stratigraphy. Geol. Correlation*, 2010, vol. 18, no. 1, pp. 1–15.

Ayer, J., Amelin, Y., Corfu, F., Kamo, S., Ketchum, J., Kwok, K., and Trowell, N., Evolution of the southern Abitibi greenstone belt based on U-Pb geochronology: autochthonous volcanic construction followed by plutonism, regional deformation and sedimentation, *Precambrian Res.,* 2002, vol. 115, pp. 63–95.

Balagansky, V.V., Main Stages in the Paleoproterozoic Tectonic Evolution of the Northeastern Baltic Shield, *Extended Absract of Doctoral (Geol.-Min.) Dissertation,* St. Petersburg: SPbGU, 2002.

Balagansky, V.V., Mints M.V., and Daly, J.S., Paleoproterozoic Lapland–Kola orogen, in *Stroenie i dinamika litosfery Vostochnoi Evropy. Rezul'taty issledovanii po programme EUROPROBE* (Structure and Dynamics of the East European Lithosphere. Results of Studies of the EUROPROBE program), Geokart/Geos: Moscow, 2006, pp. 158–171.

Bortnikov, N.S., On reliability of the arsenopyrite and arsenopyrite–sphalerite geothermometers, *Geol. Ore Deposits,* 1993, vol. 35, no. 2, pp. 177–191.

Daly, J.S., Balagansky, V.V., Timmerman, M.J., Whitehouse, M.J., de Jong, K., Guise, P., Bogdanova, S., Gorbatschev, R., and Bridgwater, D., Ion microprobe U-Pb zircon geochronology and isotopic evidence for a transcrustal suture in the Lapland–Kola orogen, northern Fennoscandian Shield, *Precambrian Res.,* 2001, vol. 105, pp. 289–314.

Daly, J.S., Balagansky, V.V., Timmerman, M.J., and Whitehouse, M.J., The Lapland–Kola orogen: Palaeoproterozoic collision and accretion of the northern Fennoscandian lithosphere, in *European Lithosphere Dynamics,* Gee, D.G. and Stephenson, R. A., Eds., *Geol. Soc. London Mem.,* 2006, vol. 32, pp. 579–598.

Davis, D.W., U-Pb geochronology of Archean metasedimentary rocks in the Pontiac and Abitibi subprovinces, Quebec, constraints on timing, provenance and regional tectonics, *Precambrian Res.,* 2002, vol. 115, pp. 97–117.

Dube, B. and Gosselin, P., Greenstone-hosted quartz-carbonate vein deposits. Mineral deposits of Canada: a synthesis of major deposit-types, district metallogeny, the evolution of geological provinces, and exploration methods, *Geol. Assoc. Can. Miner. Deposits Div., Spec. Publ.,* 2007, vol. 5, pp. 49–73.

Dube, B., Williamson, K., McNicoll, V., Malo, M., Skulski, T., Twomey, T., and Sanborn-Barrie, M., Timing of gold mineralization in the Red Lake gold camp, northwestern Ontario, Canada: new constraints from U-Pb geochronology at the Goldcorp high-grade zone, Red Lake mine and at the Madsen mine, *Econ. Geol.,* 2004, vol. 99, pp. 1611–1641.

Eilu, P., FINGOLD—a public database on gold deposits in Finland, *Geol. Surv. Finland. Rept. of Investigation,* vol. 146, 2009.

Eisenlohr, B.N., Groves, D.I., and Partington, G.A., Crustal-scale shear zones and their significance to Archaean gold mineralization in western Australia, *Mineral. Deposita,* 1989, vol. 24, pp. 1–8.

Gavrilenko, B.V., Metallogeny of Noble Metals and Diamonds of the Northeastern Baltic Shield, *Doctoral (Geol.-Min.) Dissertation,* Apatity, 2003.

Gavrilenko, B.V. and Kalinin, A.A., Mineralogical-geochemical aspects of gold and silver metallogeny of the Kola region, in *Problemy zolotonosnosti i almazonosnosti Severa evropeiskoi chasti Rossii* (Problems of the Gold and Diamond Potential of the Northern European Russia), Petrozavodsk, 1997, pp. 68–73.

Glubinnoe stroenie, evolyutsiya i poleznye iskopaemye rannedokembriiskogo fundamenta Vostochno-Evropeiskoi platformy: interpretatsiya materialov po opornomu profilyu 1-EV, profilyam 4V i TATSEIS (Deep Structure, Evolution, and Mineral Resources of the Early Precambrian Basement of the East European Platform: Interpretation of Minerals on the 1-EV, 4V, and TATSEIS Profiles) Mints, M.V., Ed., Moscow: GEOKART: GEOS, 2010, Vol. 1.

Goldfarb, R.J., Groves, D.I., and Gardoll, S., Orogenic gold and geologic time: a global synthesis, *Ore. Geol. Rev.,* 2001, vol. 18, pp. 1–75.

Gosudarstvennaya geologicheskaya karta Rossiiskoi Federatsii. Masshtab 1 : 1000000 (tret'e pokolenie). Seriya Baltiiskaya. List Q_37-Arkhangel'sk. Ob"yasnitel'naya zapiska (State Geological Map of the Russian Federation. Scale 1 : 1000000 (3rd Generation). Baltiiskaya Series. Sheet Q_37-Arkhangel'sk. Explanatory Note*),* St. Peterburg Kartograficheskaya Fabrika VSEGEI, St. Petersburg, 2012.

Groves, D.I., Goldfarb, R.J., Robert, F., and Hart, C.J.R., Gold deposits in metamorphic belts: overview of current understanding, outstanding problems, future research, and exploration significance, *Econ. Geol.,* 2003, vol. 98, pp. 1–29.

Imandra-Varzugskaya zona karelid (geologiya, geokhimiya, istoriya razvitiya) (Imandra–Varzuga Zone of Karelides (Geology. Geochemistry, History of Evolution), Gorbunov, G.I, Ed., Nauka: Leningrad, 1982.

Jensen, L.S., A new cation plot for classifying subalkalic volcanic rocks, *Ontario Div. Mines. Misc.,* 1976, Pap. 66.

Kol'tsov, A.B., Metasomatic Processes at the gold deposits in metaterrigenous complexes, *Extended Abstract of Doctoral (Geol.-Min.) Dissertation*, Sankt-Peterburg: SPbGU, 1996.

Kozlov, M.T., *Razryvnaya tektonika severo-vostochnoi chasti Baltiiskogo shchita* (Fault tectonics of the Northeasten Baltic Shield), Leningrad: Nauka, 1979.

Kretschmar, U. and Scott, S.D., Phase relations involving arsenopyrite in the system Fe–As–S and their application, *Can. Mineral.,* 1976, vol. 14, pp. 364–386.

Krogh, T.E., A low-contamination method for hydrothermal dissolution of zircon and extraction of U and Pb for isotopic age determinations, *Geochim. Cosmohim. Acta*, 1973, vol. 37, pp. 485–494.

Kuleshevich, L.V., Rybozero gold deposit in the South Vygozero greenstone belt (eastern Karelia), *Geol. Polezn. Iskop. Karelii,* 2013, vol. 16, pp. 89–101.

Ludwig, K.R., *PbDat for ms_dos. version 1.21*, *U.S. Geol. Surv. Open File Rept.,* 1991, vol. 8-542.

Ludwig, K.R., Isoplot/ex - a geochronological toolkit for Microsoft Excel, version 2.05, *Berkeley Geochronol. Center Sp. Publ.,* 1999, no. 1a.

McCuaig, T.C. and Kerrich, R., P-T-t-deformation-fluid characteristics of lode gold deposits: evidence from alteration systematic, *Ore Geol Rev.,* 1998, vol. 12, pp. 381–453.

Mineral'no-syr'evaya baza Respubliki Kareliya. Kn. 1 (Mineral–Raw Base of Karelia Republic) Mikhailov, V. P. and Aminov, V. N, Eds., Kareliya: Petrozavodsk, 2005, vol. 1.

Neumayr, P., Hagemann, S.G., and Couture, J.-F., Structural setting textures and timing of hydrothermal vein systems in the Vald'Or camp, Abitibi, Canada: implications for the evolution of transcrustal, second- and higher-order fault zones and gold mineralization, *Can. J. Earth Sci.,* 2000, vol. 37, pp. 95–115.

Neumayr, P. and Hagemann, S.G., Hydrothermal fluid evolution within the Cadillac tectonic zone, Abitibi greenstone belt, Canada: relationship to auriferous fluids in adjacent second- and third-order shear zones, *Econ. Geol.,* 2002, vol. 97, pp. 1203–1225.

Nurmi, P.A., Geological setting, history of discovery, and exploration economics of Precambrian gold occurrences in Finland, *J. Geochem. Explor.,* 1991, vol. 39, pp. 273–287.

Ojala, V.J., (ed.). *Geological Survey of Finland.* Special Paper, part 44, Espoo, 2007.

Otto, A., Dziggel, A., Kisters, A.F.M., and Meyer, F.M., The New Consort gold mine, Barberton greenstone belt, South Africa: orogenic gold mineralization in a condensed metamorphic profile, *Mineral. Deposita,* 2007, vol. 42, pp. 715–735.

Poutiainen, M. and Partamies, S., Fluid inclusion characteristics of auriferous quartz veins in Archean and Paleoproterozoic greenstone belts of eastern and southern Finland, *Econ. Geol.,* 2003, vol. 98, pp. 1355–1369.

Pozhilenko, V.I., Gavrilenko, B.V., Zhirov, D.V., and Zhabin, S.V., *Geologiya rudnykh raionov Murmanskoi oblasti* (Geology of Ore Districts of the Murmansk Area), KNTs RAN, 2002.

Simard, M., Gaboury, D., Daigneault, R., and Mercier-Langevin, P., Multistage gold mineralization at the Lapa Mine, Abitibi subprovince: insights into auriferous hydrothermal and metasomatic processes in the Cadillac-Larder Lake fault zone, *Mineral. Deposita,* 2013, vol. 48, pp. 883–905.

Smol'kin, V.F. Metamorphism of basite–hyperbasite intrusions of the Southern Varzuga Fault (Imandra-Varzuga Zone), in *Metamorfizm i metamorfogennoe rudoobrazovanie rannego dokembriya* (Metamorphism and Metamorphogenic Ore Formation of the Early Precambrian), Apatity: Kol'sk. Fil. AN SSSR, 1984, pp. 78–85.

Stacey, J.S. and Kramers, J.D., Approximation of terrestrial lead isotope evolution by a two-stage model, *Earth Planet. Sci. Lett.,* 1975, vol. 26, pp. 207–221.

Steiger, R.H. and Jager, E., Subcommission on geochronology: convention on the use of decay constants in geo- and cosmochronology, *Earth Planet. Sci. Lett.,* 1977, vol. 36, no. 3, pp. 359–362.

Timmerman, M.J. and Daly, J.S., Sm-Nd evidence for Late Archaean crust formation in the Lapland–Kola mobile belt, Kola Peninsula, Russia and Norway, *Precambrian Res.,* 1995, vol. 72, no. 12, pp. 97–107.

Vrevsky, A.B., Matrenichev, V.A., and Ruzh'eva, M.S., Petrology of komatiites from the Baltic Shield and isotope geochemical evolution of their mantle sources, *Petrology,* 2003, vol. 1, no. 6, pp. 532–561.

Witt, W.K. and Vanderhor, F., Diversity within a unified model for Archaean gold mineralization in the Yilgarn craton of western Australia: an overview of the late-orogenic, structurally-controlled gold deposits, *Ore Geol. Rev.,* 1998, vol. 13, pp. 29–64.

Translated by V. Popov